

Journal Pre-proof

Dynamic wetting of various liquids: Theoretical models, experiments, simulations and applications

Yichuan Zhang, Mingming Guo, David Seveno, Joël De Coninck



PII: S0001-8686(23)00028-3

DOI: <https://doi.org/10.1016/j.cis.2023.102861>

Reference: CIS 102861

To appear in: *Advances in Colloid and Interface Science*

Revised date: 12 February 2023

Please cite this article as: Y. Zhang, M. Guo, D. Seveno, et al., Dynamic wetting of various liquids: Theoretical models, experiments, simulations and applications, *Advances in Colloid and Interface Science* (2023), <https://doi.org/10.1016/j.cis.2023.102861>

This is a PDF file of an article that has undergone enhancements after acceptance, such as the addition of a cover page and metadata, and formatting for readability, but it is not yet the definitive version of record. This version will undergo additional copyediting, typesetting and review before it is published in its final form, but we are providing this version to give early visibility of the article. Please note that, during the production process, errors may be discovered which could affect the content, and all legal disclaimers that apply to the journal pertain.

© 2023 Published by Elsevier B.V.

Dynamic wetting of various liquids: theoretical models, experiments, simulations and applications

Yichuan Zhang^{a,b,c,*}, Mingming Guo^a, David Seveno^b, Joël De Coninck^{c,*}

^aSchool of Chemistry and Chemical Engineering, Chongqing Key Laboratory of Soft-Matter Material Chemistry and Function Manufacturing, Southwest University, Chongqing 400715, China

^bDepartment of Materials Engineering, KU Leuven, 3001 Leuven, Belgium

^cTransfers, Interfaces and Processes, Université libre de Bruxelles, 1050 Bruxelles, Belgium

Emails: zhangyichuan@swu.edu.cn (Y. Zhang); Joel.DECONINCK@umons.ac.be (J. De Coninck)

Abstract

Dynamic wetting is a ubiquitous phenomenon and frequently observed in our daily life, as exemplified by the famous lotus effect. It is also an interfacial process of utmost importance involving many cutting-edge applications and has hence received significantly increasing academic and industrial attention for several decades. However, we are still far away to completely understand and predict wetting dynamics for a given system due to the complexity of this dynamic process. The physics of moving contact lines is mainly ascribed to the full coupling with the solid surface on which the liquids contact, the atmosphere surrounding the liquids, and the physico-chemical characteristics of the liquids involved (small-molecule liquids, metal liquids, polymer liquids, and simulated liquids). Therefore, to deepen the understanding and efficiently harness wetting dynamics, we propose to review the major advances in the available literature. After an introduction providing a concise and general background on dynamic wetting, the main theories are presented and critically compared. Next, the dynamic wetting of various liquids ranging from small-molecule liquids to simulated liquids are systematically summarized, in which the new physical concepts (such as surface segregation, contact line fluctuations, etc.) are particularly highlighted. Subsequently, the related emerging applications are briefly presented in this review. Finally, some tentative suggestions and challenges are proposed with the aim to guide future developments.

keywords

dynamic wetting; theoretical models; contact line; interface; energy dissipations

1. Introduction

Wetting phenomena are ubiquitous in nature and are utilized in our daily life. Typical examples include the lotus leaf [1], water strider [2], and desert beetle [3], spider silk [4], etc. These fascinating examples are the sources of biomimetic investigations and have provided inspirations to scientists and engineers in developing multifunctional surfaces with unique wettability, like biomimetic fibers with the ability of harvesting water from air and anti-fog glasses with a curved substrate controlling the wetting behavior of water droplets, by tailoring a surface with surface tension gradients or a difference in Laplace pressure [5-8]. The significance of this topic has aroused considerable attention from the academic and industrial communities for several decades. Particularly, the popularity of this topic has witnessed a significant continuous increase in academic interests, as demonstrated by the number of research articles (Fig. 1) based on Web of Science database searching the topic “dynamic wetting”. This number should be lower limit to the published papers, since the associated keywords “wetting dynamics” and “spreading dynamics” are not included in the search (it may lead to many duplications if two keywords are also counted). It clearly suggests that the field of dynamic wetting has gathered momentum in the recent decades.

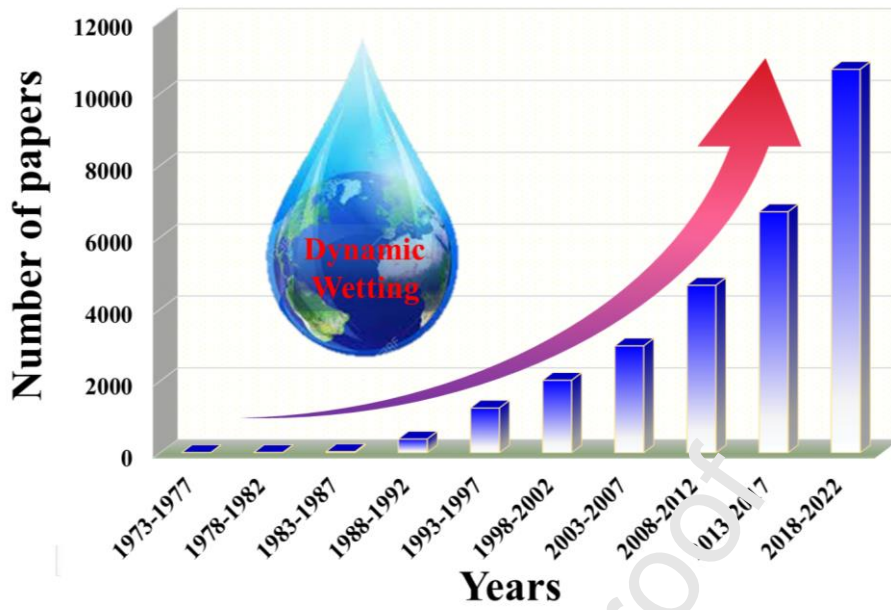


Fig. 1. Number of papers published in the recent 50 years based on the Web of Science database searching the topic “dynamic wetting” (the data are updated on 25 Oct., 2022).

When a liquid is placed in contact with a solid substrate, the liquid front moves spontaneously towards equilibrium due to the out-of-balance Young’s force. As the liquid front moves, the dynamic contact angle (θ_d) and the contact-line position (x_{CL}) relaxes towards an equilibrium state characterized by a static contact angle (θ_0). It is obvious that the contact line velocity (V) is a function of the driving force:

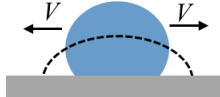
$$V = \frac{dx_{CL}}{dt} = f(\cos \theta_0 - \cos \theta_d) \quad (1)$$

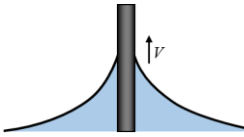
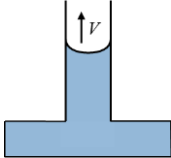
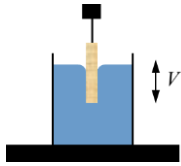
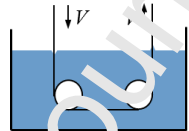
with $f(0)=0$ at equilibrium [9]. The key tenet of Eq. (1) is in the nature of the function $f(x)$. As pointed out by de Gennes [10], there are several channels of energy dissipations, each of which triggers the elaboration of different theoretical forms for the function $f(x)$. Despite the great endeavor to understand and resolve Eq. 1 in more

than half a century, we are not able to completely predict dynamic wetting for a given system. That is to say, the $f(x)$ is not a universal function based on the different channels of energy dissipations. The root may lie in the fact that the precise mechanism, *i.e.*, the function $f(x)$, by which a liquid front moves across a solid remains only partially understood.

Different experimental conditions mostly driven by the substrate geometry have been adopted to study dynamic wetting, as summarized in Table 1. As Eq. 1 suggested, the dynamic processes are thermodynamically irreversible involving energy dissipations and usually characterized by a semi quantitative relationship between θ_d and V (namely, $\theta_d \sim V$, or $\theta_d \sim Ca$, with capillary number $Ca = \eta V / \gamma$, η is the viscosity, γ is the surface tension) or spreading law ($\theta_d \sim t^m$ or radius versus $R_t \sim t^m$). As a whole, there are two types of dynamic wetting: spontaneous and forced wetting (Table 1). The typical examples of spontaneous wetting are drop spreading and capillary rise. At the moment of the liquid contacting the solid surface, the dynamic contact angle will relax towards its equilibrium value. Meanwhile, the contact line velocity decreases to zero at equilibrium.

Table 1. Most studied wetting geometries.

Wetting situations	Schematic	Categories	Measuring method	References
Drop spreading		Spontaneous wetting	Optical method	[11-14]

Capillary rise		Spontaneous wetting	Optical method	[15-17]
Capillary tube		Spontaneous wetting	Optical method	[18-21]
Wilhelmy plate		Forced wetting	Optical and/or Mechanical method	[22-24]
Coating Tape		Forced wetting	Optical method	[25-27]

The other case is forced wetting where an external force is applied to move the solid-liquid interfacial area beyond equilibrium (for example, the coating tape in Table 1). In steady state condition, the displacement rate of the moving substrate is equivalent to the contact line velocity (V) when the slip does not exist [15]. It is generally observed that advancing angles increase whereas receding angles decrease

with the increasing contact line velocity [26,28-30]. Fig. 2 illustrates the velocity-dependence of dynamic contact angle for a given system including advancing ($V > 0$) and receding ($V < 0$) velocity. Fig. 2 also exhibits contact angle hysteresis that is defined as the difference between the static advancing and static receding contact angles. The hysteresis has long been attributed to the surface roughness and/or chemical heterogeneity. Recent studies [31-33] have suggested that the contact angle hysteresis even exists on smooth homogenous solid substrates, owing to a special s-shape disjoining/conjoining pressure isotherm including electrostatic, intermolecular, and structural components [34-36]. The hysteresis can complicate both the measurement and the interpretation of dynamic wetting as it may lead to a pinning effect with subsequent unsteady motion of the contact line (so-called stick-slip motion). It should be noted that the dynamic contact angle is dependent on velocity but independent on time in forced wetting (Fig. 2), which is different from spontaneous wetting. However, forced wetting and spontaneous spreading involve the same underlying mechanisms and they can be described in an equivalent way [37]. Forced wetting is related to the dynamic balance between the relaxing tendency towards equilibrium and the external force driving the system away from equilibrium [38]. Spontaneous wetting is about the evolution towards equilibrium. Both processes are thermodynamically irreversible and energy-dissipative. These factors are evidences that both processes involve the same underlying mechanism if slip is not considered.

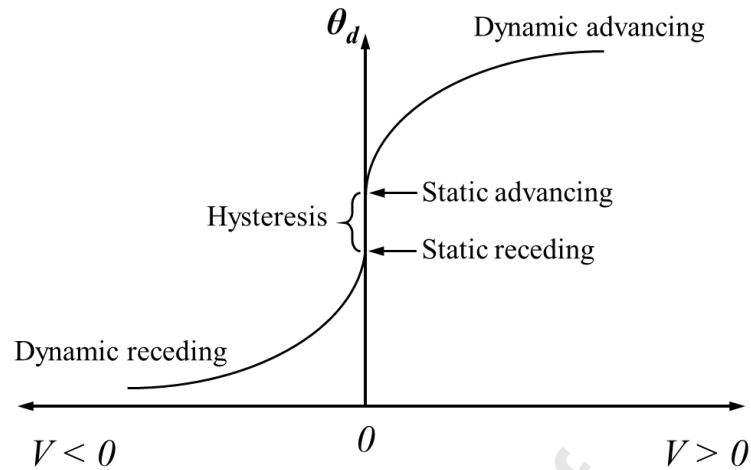


Fig. 2. Schematic illustration of the velocity-dependence of dynamic contact angle for forced wetting.

Due to the significance and complexity of dynamic wetting, most works have endeavored to understand the dynamic wetting behaviors of liquids on flat substrates, which have been summarized in many classical reviews [10,34,38-45]. These reviews have discussed the basics of dynamic wetting, the effects of the solid surface characteristics and liquid properties on dynamic wetting. However, they were limited to some specific kind of liquids, specific surface characteristics or specific theoretical approaches [41,42,44,46]. Actually, significant progress has been achieved in the recent years from both theoretical and experimental aspects where new concepts (such as surface segregation [47] and contact line fluctuation [48]) and characterization techniques, *e.g.*, tapping-mode atomic force microscopy [49] have been proposed for dynamic wetting. According to our literature survey, there is not a single comprehensive review covering the recent development of the theoretical models,

new physical concepts, a classified discussion of various liquids and their cutting-edge applications for dynamic wetting. It motivates us to thoroughly summarize the recent advances on this topic in the present review article. After the introduction, we present the two main theoretical approaches, *i.e.*, the hydrodynamic approach (HD) and the molecular-kinetic theory (MKT) and the developed models based on these two approaches. Afterwards, recent important studies investigating small-molecule liquids, metal liquids, polymer liquids and simulated liquids are described. Emerging applications are then briefly described in the following section. In the final section, a brief conclusion is drawn and some challenges and suggestions are presented. It is expected that the summarized works are most updated, sufficiently comprehensive, and representative, thereby providing a valuable reference for scientists and engineers working on this topic.

2. Theoretical models of dynamic wetting

To describe the dynamic wetting, several theoretical approaches have been proposed to predict the dynamic process or explain the observed behaviors, such as the hydrodynamic approach (HD) for viscous bending during displacement of the contact line [50-52], molecular-kinetic theory (MKT) for contact line friction dissipation in the vicinity of the contact line [38,53,54], the interface formation model (IFM) proposed by Shikhmurzaev [55,56] and the molecular self-layering model (MSLM) considering the role of the molecular shape on self-layering and its effect on the molecularly thin film viscosity [57], and some combined models incorporating HD and MKT models [58-60]. Fig. 3 briefly outlines the temporal development of

these models. It should be pointed out that Fig. 3 cannot include all many important theoretical works [50,51,61-64], like the lubrication flow approximation by Huh and Scriven [50], the MKT considering specific solid/liquid interactions formulated by Blake and De Coninck [61], etc. Concerning these theoretical approaches, except for the Shikhmurzaev model, others essentially boil down to HD and MKT (to some extent, MSLM model is also a form of MKT with the consideration of the molecular shape), and thus the two models are the most influential.

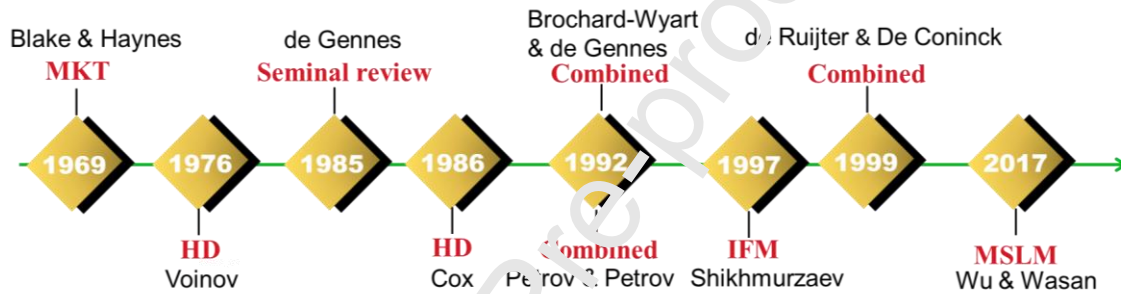


Fig. 3. The temporal development of the typical theoretical models for dynamic wetting [52,53,55,57-60,65].

2.1. Hydrodynamic approach

The HD model emphasizes the dissipation due to viscous flow within the liquid wedge during the displacement of the contact line. This model divides the moving contact line region into three relevant length scales [39,42,44,65], as shown in Fig. 4. In the macroscopic scale ($10^{-7} \sim 10^{-3}$ m, also known as "the outer region"), the gravity and/or the capillary force govern the fluid flow, which can be described by Navier-Stokes (N-S) equations with non-slip boundary conditions. The macroscopic contact angle is defined by the apparent contact angle (θ_a , as illustrated in Fig. 4)

when the moving liquid surface is extrapolated to the solid surface. In the mesoscopic scale ($10^{-7} \sim 10^{-9}$ m, also called "intermediate region"), the strongly bent interface results in a rapid change of the interface slope that is determined by viscous and capillary forces [39,44,66]. In the microscopic scales ($<10^{-9}$ m, also called "inner region"), the N-S equations with non-slip boundary conditions cannot accurately describe the contact line motion anymore [39,67] possibly due to the heterogeneity of the liquid or solid substrate, non-Newtonian effects of liquid and the related interfacial interactions at the nanoscale (these characteristics at the nanoscale are not considered in the HD model). The microscopic contact angle is defined as the real contact angle (θ_m , as illustrated in Fig. 4). As is now well known, the classical HD model cannot lead to a physically acceptable solution to describe the viscous flow within a liquid wedge (the inner region, as shown in Fig. 4). This is because the application of the no-slip condition to describe the fluid flow in the vicinity of the contact line gives rise to an energy dissipation that is logarithmically diverging [39,50]. Voinov [52] suggested that this singularity can be dealt with artificial truncation of the solution at the molecular scale and it leads to the breaking down of the continuum description. Alternatively, the flow equations and boundary conditions containing a precursor film [68,69], slip conditions [50], surface roughness [70], etc. [45,71-75], also have been modified to relieve the contact line singularity. Details of the different hypothesized mechanisms tackling the diverging issue have been summarized in the reviews by Bonn et al.[39] and Lu et al. [42]. As pointed out by Bonn et al.[39], scarcely any existing experimental results would pinpoint these

hypothesized mechanisms.

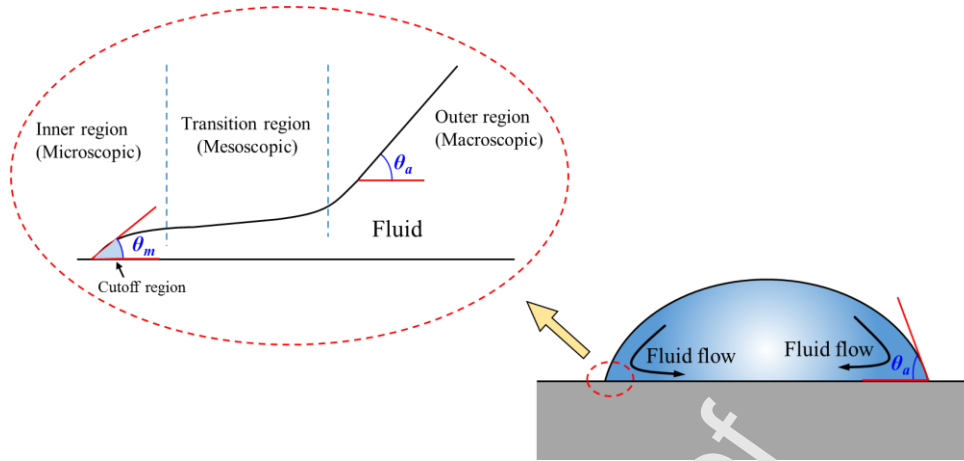


Fig. 4. Schematic of a liquid droplet on a flat surface illustrating the three regions depicted by the HD model.

The HD model [38,52,57,65] predicts that the variation of the dynamic contact angle can be written in terms of the capillary number Ca as

$$\chi(\theta_d) - \chi(\theta_m) = Ca \ln\left(\frac{L}{L_s}\right) \quad (2)$$

with $\chi(\theta) = \int_0^\theta \frac{x - \sin x \cos x}{2 \sin x} dx$. The microscopic contact angle θ_m is usually assumed to be the static contact angle θ_0 or equilibrium contact angle θ_{equ} , η is the liquid dynamic viscosity (Pa.s), L_s and L are appropriately chosen macroscopic and microscopic length scales, respectively. Normally, L_s and L are referred as the slip length (m), and a characteristic length scale of the liquid (m). In practice, the term $\ln(L/L_s)$ is usually treated as an adjustable free parameter when fitting experimental data. $\ln(L/L_s)$ is estimated to be of the order of 10 in Cox's analysis [65] in which L is set to be 10 μm (assume the approximate distance from the wetting line) and L_s is set to be 1 nm (the order of molecular size). Larger values of $\ln(L/L_s)$ are also reported for

other systems [66,76].

Concerning θ_m in Eq. 2, it is usually assumed to be governed by short-range intermolecular forces and retains its equilibrium contact angle θ_{equ} (in practice, θ_{equ} is usually equal to θ_0). This assumption was supported by molecular dynamic simulations of the contact line motion conducted by Thompson and Robbins [67] who found that θ_m is constant and equal to the equilibrium contact angle while the velocity dependence of θ_a follows the HD equation. However, it also was pointed out by other researchers that θ_m may be velocity-dependent [40,52,55]. Recently, this statement has gradually confirmed experimentally thanks to the developments of modern characterization techniques. In this respect, Wang's group [49,77,78] presented important experimental evidence to improve our understanding of θ_m by a state-of-the-art tapping-mode atomic force microscopy (T-M AFM). They observed a convex shape about 20 nm from the substrate for a glycerol droplet when extending the interface profile to the substrate (Fig. 5a) [77]. Besides, the bending curvature of the convex shape increases with the advancing spreading velocity (Fig. 5b). The authors claimed that the experimental observation of a shoe-tip-like bending region within 20 nm of the substrate could end the long-standing debate on the spreading velocity dependence of θ_m . However, the authors recognized that the convex bending cannot be seen in every completely wetting case with a slightly concave shape (such as silicon oil on mica) that is consistent with the θ_m assumption (θ_m is assumed to be constant) in HD approach. Therefore, the question of velocity-dependence of θ_m seems still open, as (i) the contact-line velocity is extremely low in their work [77]

and (ii) the convex or concave shape of the liquid wedge in a droplet for θ_m is unknown at the nanoscale in most cases. A similar method was applied to dewetting [49]. θ_m is extracted by linear fitting of the data (Fig. 5c) within 10 nm thickness from the receding contact line and it was found that θ_m decreases with the receding velocity [49]. The authors supposed that the local frictional dissipation (Fig. 5d) that is usually neglected in HD approach is responsible for the deviation of θ_m from the equilibrium angle.

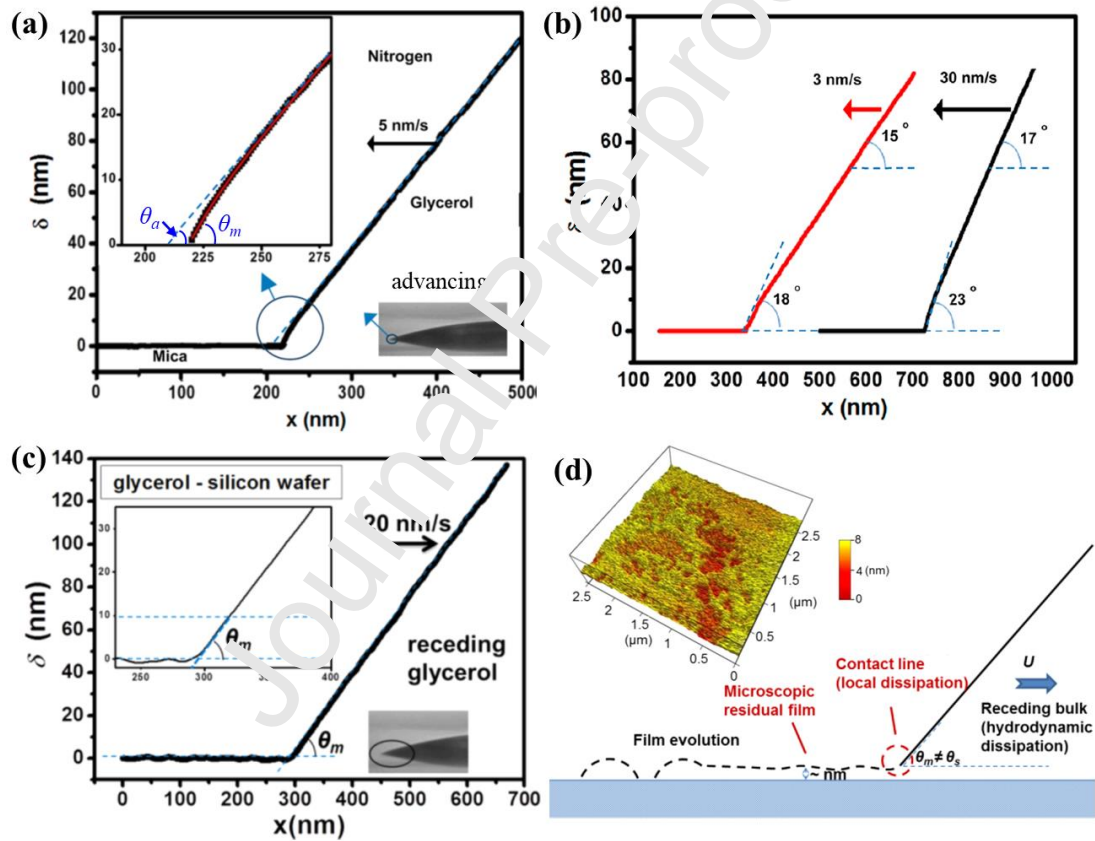


Fig. 5. (a) Nanoscopic profile near the advancing contact line of a glycerol droplet; (b) Comparison of profiles at two velocities for glycerol liquid; (a, b) Reproduced with permission [77]. Copyright 2014, American Chemical Society; (c) Nanoscopic profile near the receding contact line of glycerol liquid; (d) Schematic diagram of nonvolatile liquid structure at the receding contact line on partially wetted solid; (c, d)

Reproduced with permission [49]. Copyright 2016, American Chemical Society.

When $\theta_d < 3\pi/4$, $\chi(\theta)$ in Eq. 2 can be integrated to be approximately $\theta^3/9$.

Therefore, Eq. 2 can be rewritten as

$$\theta_d^3 - \theta_0^3 = 9Ca \ln\left(\frac{L}{L_s}\right) \quad (3)$$

or equivalently

$$V = \frac{\gamma}{9\eta} (\theta_d^3 - \theta_0^3) \left[\ln\left(\frac{L}{L_s}\right) \right] \quad (4)$$

Another representative HD approach based on the lubrication approximation developed by Brochard-Wyart and de Gennes [60] led to Eq. 5. It describes the spreading behaviors of the known droplet shapes (wedge-shaped contact line region).

This equation is

$$\theta_d (c_a^2 - c_0^2) = 6 \ln\left(\frac{x_{\max}}{x_{\min}}\right) Ca \quad (5)$$

where the cut off x_{\min} is comparable to a molecular size below which the continuum theory breaks down, and x_{\max} is a macroscopic cut off that is usually set equal to the capillary length [79].

2.2 Molecular-kinetic Theory

The MKT proposed by Blake and Hayes [38,53,54] concentrates on the frictional processes occurring in the vicinity of the advancing or receding contact line. The basic tenet is that the motion of the contact line is determined by the molecular adsorption or desorption processes based on the activated rate viewpoints invoking

of the sinh function is small, Eq. 6 can be simplified to

$$V = \frac{\gamma}{\zeta} (\cos \theta_0 - \cos \theta_d) \quad (7)$$

where ζ (Pa·s) is the contact line friction per unit length of the contact line given by

$$\zeta = k_B T / (\kappa^0 \lambda^3) \quad (8)$$

ζ is an index of the energy dissipation resulting from the movement of the contact line across the solid. Concerning the validity of Eq. 7, Fig. 7 compares the predictions given by the full MKT model (Eq. 6) and the linear model (Eq. 7). It suggests that the accuracy of the linear model is acceptable when the contact line velocity is low enough.

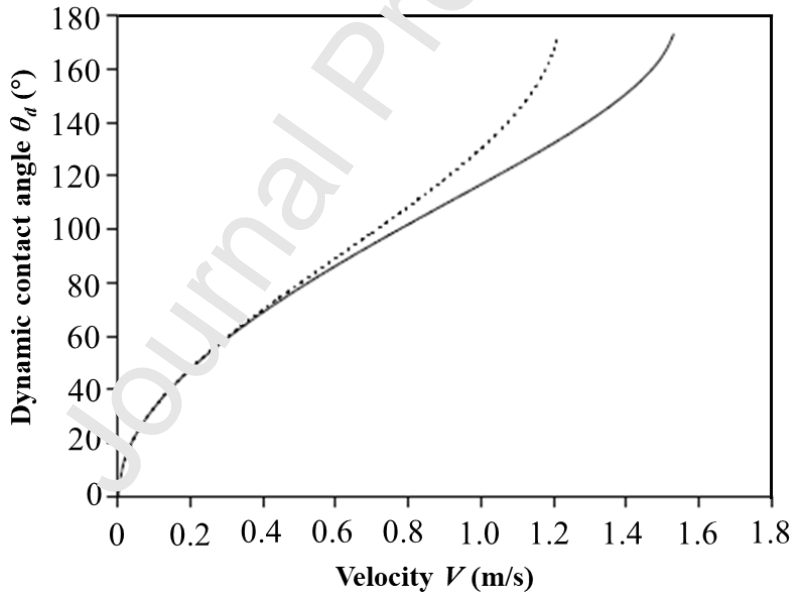


Fig. 7. Comparison of the general MKT (solid line for Eq. 6) and linear MKT (dotted line for Eq. 7) models with $\kappa^0 = 10^9 \text{ s}^{-1}$, $\lambda = 5 \text{ \AA}$, $T = 300 \text{ K}$, $\gamma = 20 \text{ mN/m}$ and $\theta_0 = 0^\circ$.

The image is reproduced from Seveno [82] with permission.

Blake [54] suggested that the molecular displacements are retarded not only by

interfacial interactions with the solid but also by viscous interactions with neighboring liquid molecules in the vicinity of the contact line. That is to say, the total activation free energy ΔG_w^* can then be written as the sum of solid/liquid interaction and viscous interactions of liquid, *i.e.*, $\Delta G_w^* = \Delta G_s^* + \Delta G_{vis}^*$, where ΔG_s^* and ΔG_{vis}^* are respectively solid/liquid interaction and viscous interactions of liquid molecules. Later, Blake and De Coninck [61] defined the specific activation free energy of wetting (unit area) $\Delta g_w^* = n\Delta G_w^*/N_A$, the surface interaction component $\Delta g_s^* = n\Delta G_s^*/N_A$ and the viscous component $\Delta g_{vis}^* = n\Delta G_{vis}^*/N_A$, with N_A being Avogadro's number. In this way, the role of liquid viscosity is directly taken into account in the MKT model [61] with the expression below

$$\kappa^0 = \frac{k_B T}{\eta v_L} \exp\left(-\frac{\Delta g_s^*}{nk_B T}\right) \quad (9)$$

where v_L is the volume of the unit of flow. Blake and De Coninck [61] suggested that Δg_s^* could be approximated by the reversible work of adhesion $W_a = \gamma(1 + \cos \theta_0)$, yielding

$$\zeta = \eta \left(\frac{v_L}{\lambda^3}\right) \exp\left(\frac{\lambda^2 W_a}{k_B T}\right) \quad (10)$$

or equivalently

$$\ln\left(\frac{\zeta}{\eta}\right) = \frac{\lambda^2 W_a}{k_B T} + \ln\left(\frac{v_L}{\lambda^3}\right) \quad (11)$$

It indicates that ζ is proportional to η and has an exponential dependence on W_a . The dependence has been validated experimentally [83]. In addition to ζ , they further [84] predict the contact line velocity V is inversely proportional to η and depends with a negative exponent on W_a . The detailed mathematical derivations of Eq. 9~11 can be

found in the works of Blake and De Coninck [54,61,84]. In this way, the roles of the liquid viscosity and the solid/liquid interfacial interactions are taken into account, which is an important step to extend the MKT. Later, they [81] summarized a very large set of dynamic wetting data spanning 9 decades of viscosities and confirmed the linear link between ζ and η in a nearly perfect agreement with Eq. 10 in Fig. 8a. They distinguished the dependence of $\ln\zeta$ upon Wa by the lines A, B and C (Fig. 8b) and 85% of all of the collected data lie between lines A and C. Based on these statistics, a semi-empirical approach was proposed

$$\ln\left(\frac{\zeta}{\eta}\right) \sim \alpha \cdot \frac{\lambda^2 Wa}{k_B T} + \ln\left(\frac{v_f}{v_{f,0.3}}\right) \quad (12)$$

where α is a correction parameter with $\alpha = 0.51 \pm 0.082$ which collates numerous data of dynamic wetting. Eq. 12 seems more universal since systematic underestimation of n arising from the roughness and heterogeneity of real solid surfaces is taken into account.

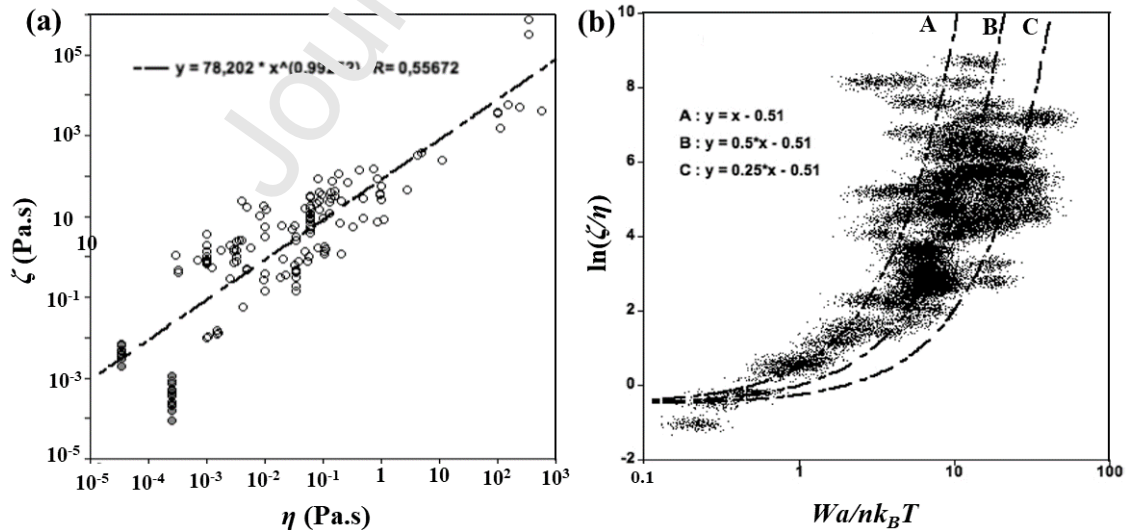


Fig. 8. (a) Plots of ζ versus η with the associated trend-line for the collated publications. (b) Clouds of 200 points in the collated publications using random

values of ζ , η , λ , and Wa with Gaussian distributions. Reproduced with permission [81]. Copyright 2013, American Chemical Society.

2.3 Comparison of the HD and MKT models

Since HD and MKT are the two main theoretical approaches to describe dynamic wetting, it is necessary to compare their pros and cons. Table 2 summarizes the differences between the HD and MKT models. The dynamic wetting is treated with macroscopic flow process in the HD model, whereas the statistical processes at the molecular scale are considered in the MKT model. The θ_0 and $\ln(L/L_s)$ are treated as adjustable parameters for HD model whereas the adjustable parameters contain θ_0 , λ , and κ^0 in the MKT. These parameters are obtained by curve-fitting procedures on basis of experimental or simulation data. It should be pointed out that θ_0 is not a mandatory adjustable parameter for HD or MKT, and it can also be obtained and treated as an input parameter. Besides, the parameters λ and κ^0 cannot be obtained experimentally easily although λ is supposed to be a certain fraction of the liquid molecule size or substrate solid inter spacing (λ is related to the cubic root of the molecular volume of the liquid [46] or the lattice spacing of the solid [81]). In sharp contrast, an advantage of HD is that the parameter L_s can be measured independently in the experimental techniques (for example by the velocimetry technique [85-88]), which can help to verify L_s values obtained by the curve-fitting. The advantage of the MKT is the microscopic insight into the interpretation of the contact line movement, without the need to introduce boundary conditions to release the mathematical

singularity brought by the HD model. The HD model neglects the local frictional dissipation in the vicinity of the contact line. However, Deng et al. [49] suggested that the ubiquitous existence of a residual film of nanometer thickness during dewetting is a clear evidence of the role of the local frictional dissipation. In the MKT model, the contact line frictional dissipation is the dominating channel of energy dissipation. The viscous effect was not taken into account in the initial MKT model (Eq. 6) [53]. The viscous effect was considered by the influence of viscosity on the jump frequency (Eq. 9) in the modified MKT model.

Table 2. Comparisons of the MKT and HD models.

Models	HD model	MKT model
Theoretical basis	Navier-Stoke equation	Eyring theory
Equations	$V = \frac{\gamma}{9\eta} (\theta_d^3 - \theta_0^3) \left[\ln \left(\frac{L}{L_s} \right) \right]^{-1}$	$V = 2\kappa^0 \lambda \sinh \left(\frac{\gamma (\cos \theta_0 - \cos \theta_d)}{2nk_B T} \right)$
Adjustable parameters	θ_0 and $\ln(L/L_s)$ (or L and L_s)	θ_0 , λ , and κ^0
θ_m	$\theta_m = \theta_0$ (assumption)	θ_m is V -dependent
Dissipation	Viscous bending	Contact line friction dissipation
Dimension	Macroscopic flow	Molecular desorption/absorption

One may realize that MKT does not discuss slip that may arise in the flow of liquid in Table 2. Actually, this parameter has been considered into the recent work of Blake et al. [89]. They computed the flow patterns of forced wetting (Couette flow, Fig. 9a) and spontaneous drop spreading (Fig. 9b), and found that the contact-line friction for the spontaneous process (no slip in their work) is clearly higher to the one

obtained for forced wetting (strong slip in their work). In addition to the capillary force $f_w = \gamma(\cos\theta_0 - \cos\theta_d)$, the shear stress stemming from the slip velocity V_{slip} acts on the whole solid-liquid interface, including the contact line, and therefore an extended MKT theory including slip with the additional term was proposed

$$V = 2\kappa^0 \lambda \sinh\left(\frac{\gamma(\cos\theta_0 - \cos\theta_d) + \zeta V_{slip}}{2nk_B T}\right) \quad (13)$$

It indicates that the shear stress together with surface tension promotes dynamic wetting and thus reduces velocity-dependence of the dynamic contact angle.

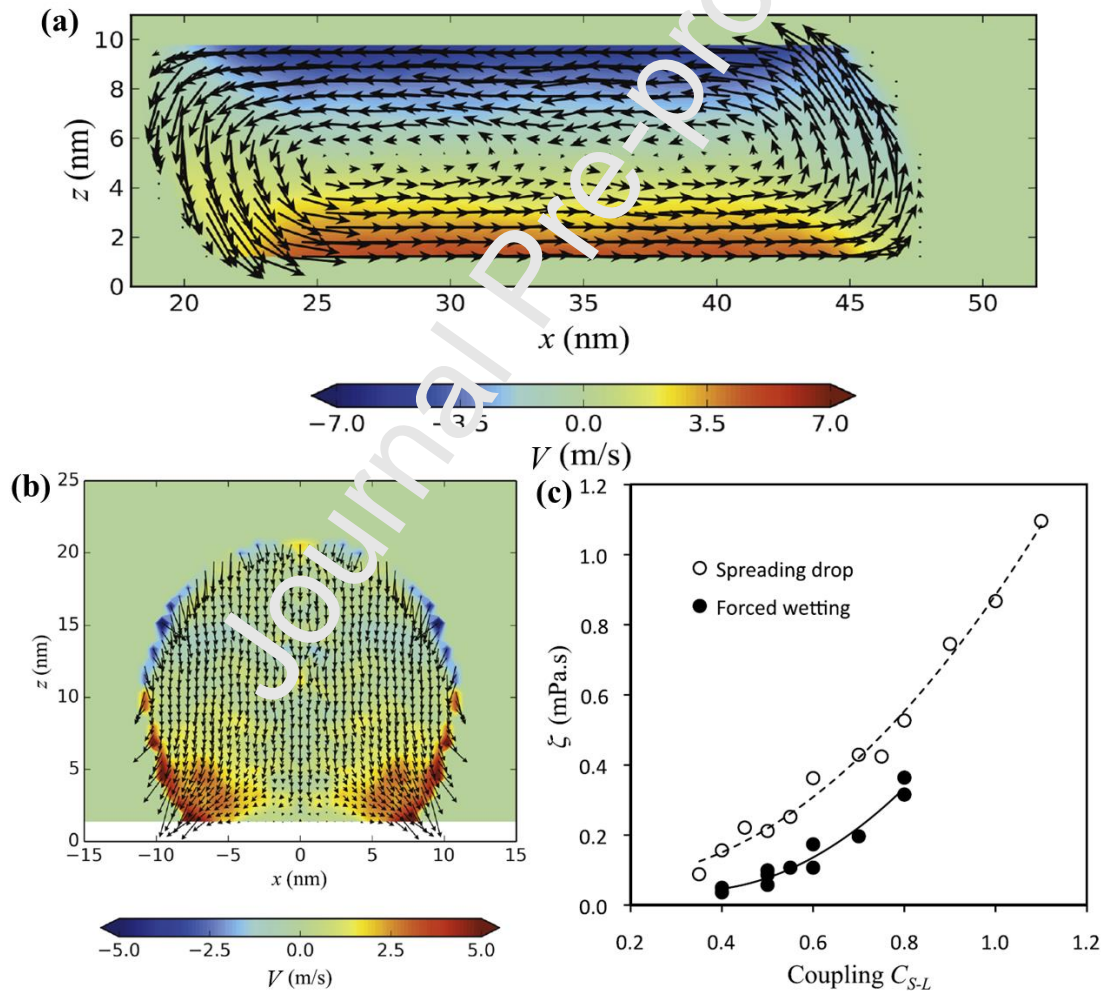


Fig. 9. Flow patterns of (a) a forced wetting with $V_{Plate} = 10$ m/s and (b) a spontaneous spreading drop; (c) the comparison of the contact line friction ζ for forced wetting and spreading drops at different the solid-liquid coupling C_{S-L} . Reproduced with


permission [89]. Copyright 2015, American Institute of Physics.

Besides, the suitability of the HD and MKT models to predict wetting dynamics has been compared and debated in the literature. Blake, Seveno, Hoffman et al. [26,38,90-92] suggested that both HD and MKT can still model successfully a given set of dynamic wetting data in several cases simultaneously, but Paneru, Sedev, and Lu et al. [42,46,93] concluded that the HD model can better describe spreading dynamics of a droplets with low contact line velocity (or small dynamic contact angle), whereas the spreading dynamics are more compatible with the MKT for high contact line velocity (or large dynamic contact angle). The work of Paneru et al. [93] is a typical example to support this argument. In their work, the contact line frictional dissipation dominates when the initial contact angle ($\sim 150^\circ$) is large and spreading speed is high in the early stages. Viscous dissipation dominates the wetting process when the dynamic contact angle is smaller in the later spreading stages. This conclusion seems to agree with the de Ruijter combined model (reviewed in the next section) [59], in which the MKT holds for the wetting dynamics at the early stage (high velocity, large contact angle) and the HD holds at late stage (low velocity, small contact angle). However, Davis et al. [94,95] argued HD tend to better describe higher contact line velocity whereas MKT are relevant in smaller contact line velocity. This opposite argument also receives some support [96-98].

When the HD and MKT models are applied to the spreading of drops with small dynamic contact angle θ_d and static contact angle $\theta_0=0$, both HD and MKT models

lead to simple scaling laws, as summarized in Tables 3 and 4, for θ_d and dynamic base radius R_t (or dynamic height y_t) as a function of time t . These scaling laws are dependent on the substrate geometries due to the Laplace pressure arising from different radii of curvatures. These relations for flat, pore and fiber geometries have been verified by experiments [15-17,99,100] and molecular dynamics simulations [101,102]. There are also some reported results deviating from the predictions of scaling law due to the effect of gravity, substrate surface contamination or surface roughness [103-105]. Tables 3 and 4 suggest that the similarity of the scaling laws for flat and pore geometries, making it quasi impossible to distinguish between HD and MKT models experimentally. That is an important reason why the hydrodynamic and molecular descriptions can be both relevant for the same experimental data in many cases [91,106]. On the other hand, comparing to flat and pore geometries, the fiber geometry presents relatively obvious differences. It implies that this geometry may be the best option when the disipation regimes have to be unambiguously distinguished.

Table 3. Scaling law $\theta_d \sim t^m$ for of HD and MKT models for different substrate geometries.

Geometry	Schematic	$m_{1,MKT}$	$m_{1,HD}$	Difference of power	References
Flat		-3/7	-3/10	0.13	[38,51,107]

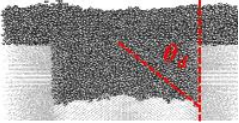
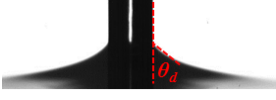
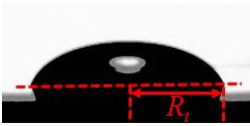
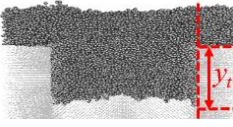
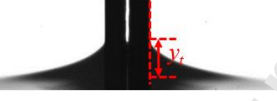
Pore		-1/4	-1/6	0.08	[102]
Fiber		-1	-1/2	0.5	[17,28]

Table 4. Scaling laws $R_t \sim t^{m_2}$ (or dynamic height $y_t \sim t^{m_2}$) for of HD and MKT models for different substrate geometries.

	Schematic	$m_{2,MKT}$	$m_{2,HD}$	Difference of power	References
Flat		1/7	1/10	0.04	[38,108]
Pore		1/2	1/2	0	[109,110]
Fiber		-1	-1/2	0.5	[16,28]

2.4 Combined models

It is often impossible to settle which of the MKT and HD is more appropriate for the given system [26,38,90-92]. Given that the two approaches are in play at different scales, the molecular and hydrodynamic ones may be complementary. Therefore, the point of view that both frictional and viscous dissipations simultaneously play an important role has gained increasing ground. The standpoint triggers different approaches to combine the HD and MKT models.

2.4.1. Petrov combined model

In Petrov's approach, Petrov and Petrov [58] considered that the microscopic contact angle θ_m appearing in the HD approach (Eq. 2) is the dynamic contact angle θ_d of the MKT model. Therefore, a combined model (Eq. 14) is formulated by simply substituting the macroscopic contact angle expression given by the MKT into the microscopic contact angle in the HD model, yielding an equation with three adjustable parameters, λ , κ_0 and $\ln(L/L_s)$,

$$\theta_d^3 = \arccos^3 \left\{ \cos \theta_0 - \frac{2k_B T}{\lambda^2 \gamma} \ln \left[\frac{V}{2\kappa^0 \lambda} + \sqrt{\left(\frac{V}{2\kappa^0 \lambda} \right)^2 + 1} \right] \right\} + 9 \frac{\nu}{\gamma} \ln \left(\frac{L}{L_s} \right) \quad (14)$$

They presented the advantage of this combined approach in the case of receding meniscus of aqueous glycerol solutions over the individual MKT and HD model [58]. However, Ranabothu et al. [111] suggested that this combined model (Eq. 14) does not present a significant advantage and produces similar fitting results with the MKT model (Eq. 6) in terms of advancing meniscus (using simple liquids such as water, glycerin, etc.). Very recently, the utility of the Petrov combined model (Eq. 14) has been demonstrated by Fernández-Toledano et al. [112] through molecular dynamic simulations in which they clarified that the velocity-dependence of θ_m is well described by MKT and the dynamic behavior of the apparent dynamic contact angle follows the HD model [112]. Their further simulation work [113], based on this combined model, reveals that viscous bending plays a comparatively minor role at the advancing meniscus, but dominates at the receding one.

When the dynamic contact angle is close to equilibrium and the linear MKT model (Eq. 7) is valid, Petrov combined model can also be simplified (Eq. 15)

$$\theta_d^3 = \arccos^3 \left[\cos \theta_0 - \frac{V\zeta}{\gamma} \right] + 9 \frac{\eta V}{\gamma} \ln \left(\frac{L}{L_s} \right) \quad (15)$$

The linear Petrov combined model was tested by Seveno et al. [91], who found the distributions of free parameters ζ and $\ln(L/L_s)$ are narrow and physically acceptable.

2.4.2. de Ruijter combined model for flat geometry

Different from the Petrov combined model, de Ruijter et al. [59] took the viscous and frictional dissipations into account simultaneously. They adapted a standard mechanical approach to the dynamics of mechanical dissipative systems, in which the driving force is balanced by the rate of dissipation function. An equation for a spreading drop was then derived,

$$V = \frac{\gamma(\cos \theta_0 - \cos \theta_d)}{\zeta + 6\eta\Phi(\theta_d)\ln(R_t/a)} \quad (16)$$

with $\Phi(\theta_d)$ a geometrical term which relates to the base radius R_t of the drop and its volume (Vol). The parameter a is a cutoff value. Without this value, similar to the original HD model, the viscous dissipation diverges, since the velocity at the symmetry axis of the droplet has a singularity. An important conclusion of the de Ruijter combined model is that a contact line friction regime precedes the viscous regime that becomes dominant when the dynamic contact angle is close to its equilibrium value. De Coninck et al. [114] pointed out this identification of MKT and HD regimes is important to assess the influence of the different parameters (surface tension, viscosity, friction) on the dynamic wetting. The subsequent work of de Ruijter et al. [108] confirmed this conclusion as shown in Fig. 10a. It indicates that, as spreading progresses, a switch of the time-dependent power, from MKT regime (R_t

$\sim t^{1/7}$) to HD regime ($R_t \sim t^{1/10}$), is expected. It offers us an understanding of the relative importance of the viscous and frictional dissipation channels at different spreading stages. Besides, the de Ruijter combined model is also used to assess the influence of ζ and η with respect to the two dissipation channels [115]. As shown in Fig. 10b, if $\zeta \ll \eta$, viscous bending is the leading channel of dissipation during most of the spreading, whereas $\zeta \gg \eta$, the contact line friction between the liquid and solid is predominant.

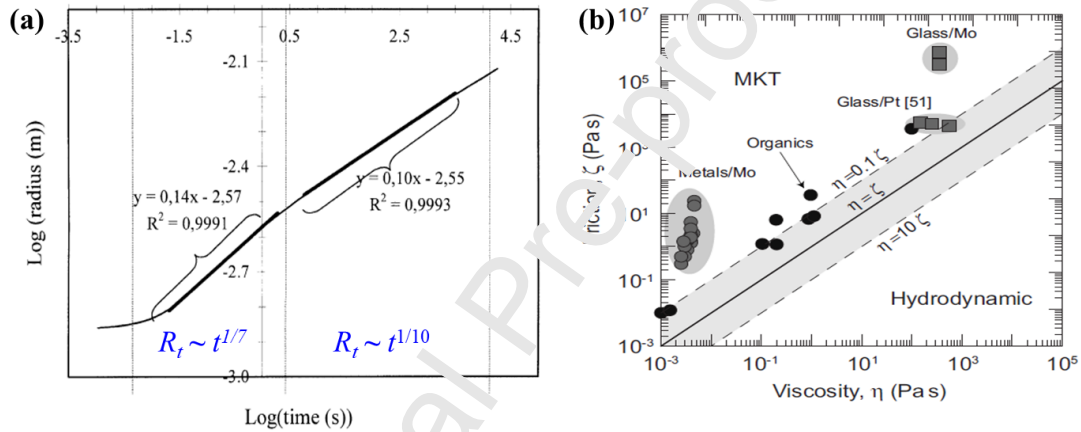


Fig. 10. (a) Predicted drop base radius dynamics showing the transition from a contact line friction dissipation to a viscous dissipation dominated process [59]. Reproduced with permission [59]. Copyright 1999, American Chemical Society. (b) Relative importance of the viscous and frictional dissipation channels for different liquids [115]. Reproduced with permission [115]. Copyright 2007, American Physical Society.

2.4.3. de Ruijter combined model for fiber geometry

As described above, the substrate geometry should be taken into account ($\Phi(\theta_d)$ in Eq. 16) when the de Ruijter combined model is applied. Thus, Seveno et

al. [101] extended this model to a fiber geometry. The relationship between dynamic contact angle θ_d , dynamic meniscus height y_t and the contact line velocity V on a fiber with radius r_0 (see the schematic in Table 3 and 4) is given by

$$V = \frac{dy_t}{dt} = \frac{\gamma(\cos\theta_0 - \cos\theta_d)}{\zeta + \frac{6\eta}{\theta_d} \ln\left(\frac{x_{\max}}{x_{\min}}\right)} \quad (17)$$

The physical meanings of x_{\max} and x_{\min} are the same as previously (see Eq. 5). x_{\max} is of the order of millimeters and x_{\min} is of molecular size [79]. The variation of θ_d is

$$\frac{d\theta_d}{dt} = \frac{\gamma(\cos\theta_0 - \cos\theta_d)}{\zeta + \frac{6\eta}{\theta_d} \ln\left(\frac{x_{\max}}{x_{\min}}\right)} \left[\frac{\partial y_t(r_0)}{\partial \theta_d} \right]^{-1} \quad (18)$$

For small values of θ_d and $\theta_0 = 0^\circ$ with the Taylor approximation of trigonometric function [101], Eq. 18 can be simplified as

$$\frac{d\theta_d}{dt} \approx \frac{\gamma\left(\frac{\theta_d^2}{2r_0}\right)}{\zeta + \frac{6\eta}{\theta_d} \ln\left(\frac{x_{\max}}{x_{\min}}\right)} \quad (19)$$

Whenever there is no friction at the contact line, it leads to

$$\theta_d \propto t^{-1/2} \quad (20)$$

and for the other case with a small viscosity, it gives

$$\theta_d \propto t^{-1} \quad (21)$$

These scaling laws were validated numerically and experimentally [16,17,99,101], and have been summarized in Table 3.

2.5. Shikhmurzaev model

Shikhmurzaev [55,56] proposed that the surface tensions at the moving interface deviate from their equilibrium values. In its simplified form, this model predicts the

relationship between the dynamic contact angle and the contact line velocity for the system with small capillary and Reynolds numbers,

$$V = \frac{\gamma}{\eta S_c} \left[\frac{\left[1 + (\cos \theta_0 - \sigma_{sg})(1 - \rho_G^s) \right] (\cos \theta_0 - \cos \theta_d)^2}{4(\cos \theta_0 + B)(\cos \theta_d + B)} \right]^{1/2} \quad (22)$$

where S_c and B is a dimensionless parameter with complex formulas that are related to the liquid surface properties [91]; σ_{sg} the dimensionless surface tension of the liquid/gas interface; ρ_G^s is the dimensionless equilibrium surface density of liquid/gas interface. This model was applied to forced wetting with a wide range of liquid viscosities and it was concluded that dynamic wetting can be described as a process of the disappearance of liquid/gas interface and the formation of liquid/solid interface as the liquid rolls over the solid substrate [26]. Heshmati and Piri [116] compared experimental capillary rise data with the Shikhmurzaev model and it showed a good agreement with the experimental velocity-dependent dynamic contact angles at low and moderate velocities in glycerol and water systems, but always over-predicted the experimental values at higher velocities. Indeed, Shikhmurzaev approach has received dogged oppositions from other researchers [117,118] and it is still highly debatable. Perhaps because of the debate, not many papers have considered this model to clarify the physical mechanism of various systems.

2.6. Molecular self-layering model

The liquid molecules may be self-layered at the liquid/solid interface, which results in a local fluctuation of density, viscosity, and fluidity of the liquids. This

fluctuation is less and less apparent away from the solid wall till local density becomes identical with the bulk one usually after around 5 layers (Fig. 11a). If a layered molecularly thin film exists ahead of the moving main meniscus, the layered wetting film has a different viscosity due to the self-layering and confinement of the liquid molecules (Fig. 11b). Similar to MKT, Wasan et al. [57,119] proposed that the driving force $\gamma(\cos\theta_0 - \cos\theta_d)$ is balanced by the viscous force $\eta_f V$ in the layered film and yielded

$$\gamma(\cos\theta_0 - \cos\theta_d) = \eta_f V \quad (23)$$

where $\eta_f = \exp\left(\frac{2\gamma}{n_l k_B T}\right) \eta$ is the viscosity in the self-layering wetting film, and other parameters are identical with those in MKT. Wasan et al. [57,119] pointed out n_l is the number of molecules per unit area that is dependent on the shape of liquid molecules (for example, $n_l = 1/\sigma^2$ for spherical molecules with σ the effective diameter). They verified this model by performing capillary rise dynamic experiments with liquids consisting of spherical, cylindrical, and disk shape molecules and concluded that the liquid molecule shapes play a key role. One may note that Eq. 23 is another form of linear MKT (Eq.7). Furthermore, the molecular self-layering model is limited to the liquid/solid system with a very small θ_m and cannot apply to systems with large θ_m since the wetting film does not exist ahead of the moving meniscus.

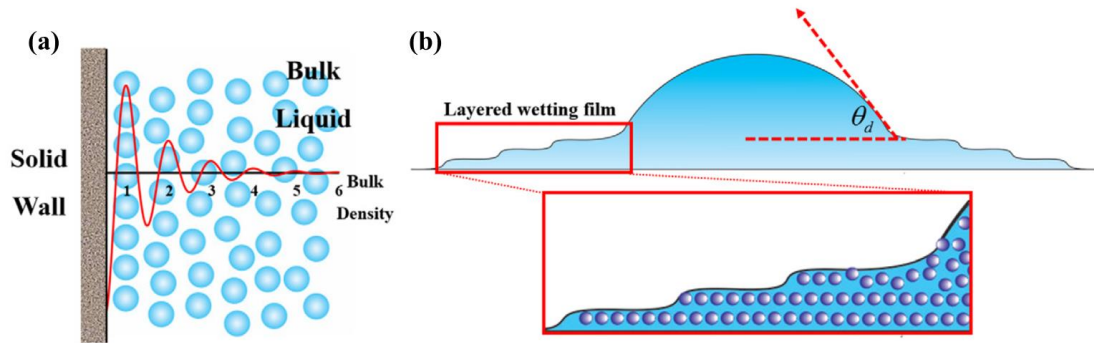


Fig. 11. (a) Self-layering of liquid molecules close to solid wall, the fluctuation of local liquid density is illustrated in the oscillatory red curve; (b) Spreading of a moving meniscus on a molecularly smooth flat surface where the molecules are well-ordered close to solid surface and gradually disordered with increasing distance from solid surface. Reproduced with permission [57], Copyright 2017, Elsevier.

3. Dynamic wetting of liquids

The suitability of the models outlined above in describing the representative behaviors of dynamic wetting is examined in this section. These cases are selected to represent the success and limitations of each model and the physicochemical properties of liquids involved are discussed. Very recent review papers [34,120] and a book chapter [121] have already comprehensively considered the effects of evaporation in the vicinity of contact line, and it is then not developed in this current review to avoid duplication.

3.1. Small-molecule liquids

The simple molecular structures and environmental stability of small-molecule liquids enable us to easily tailor their physical properties (surface tension and viscosity) and hence the wetting dynamics of small-molecule liquids have been

studied more extensively than other liquids. In general, when a liquid initially contacts a solid surface in air, inertia dominates the wetting dynamics prior to capillarity. Therefore, the effect of inertia is usually first identified by a scaling law of $R_t \sim t^{1/2}$ for the flat substrate [122,123] or $y_t \sim t^{1/2}$ for the fiber substrate [17,105], making sure the wetting process under study is inertia-free. It may be noted that the wetting dynamics in the inertia-dominated regime is considered to be independent of the hydrophobicity or wettability of the solid surface and the droplet size [11]. After the elimination of inertia, the dynamics of capillarity-dominated regime is then analyzed. For example, Seveno et al. [91] compared the spreading dynamics of squalane and n-dibutyl phthalate (DBO) on flat glass surface or a polymer film to various models (HD, MKT, Petrov, De Ruijter models, etc.). They found that all the considered models are applicable in describing spreading dynamics and concluded that it is difficult to make reliable claims as to which is best model for a given system. They pointed out that the claims should be treated with caution especially when the data sets span over a limited contact-line velocity range and the fitting procedure are less-stringent. Qiu et al. [124,125] also performed studies of wetting dynamics of small-molecule liquids (water, diiodomethane, etc.) on carbon fibers based on the Wilhelmy method and found that the dominated dissipation channel of these liquids is the contact-line friction (Eq. 7).

In contrast to the common small-molecule liquids above, ionic liquids (ILs), usually comprising bulky organic cations and organic or inorganic anions, are a unique family of molecular liquids (called "organic salts" or "molten salts") with low

melting points (usually below 100 °C) [126]. The use of ILs has borne fruit in improving the performance of many devices like supercapacitors, lubrication and thermoelectrics [127]. Ralston and co-authors [127-129] performed a series of interesting and important works on the dynamic wetting of ILs. Specifically, they investigated the wetting behaviors of two kinds of imidazolium-based ILs (anions: BF_4 and NTf_2) and found that the applicability of the HD model is rather limited (Fig. 12a) whereas their dynamic wetting behaviors can be adequately described by MKT (Fig. 12b) [128]. They further analyzed the wetting behavior by plotting the W_a dependence of $\ln(\zeta/\eta)$, as shown in Fig. 12c. The v_L values extracted from the linear curve and Eq. 10 is $0.19 \pm 0.05 \text{ nm}^3$ that is the same order of magnitude as the molecular volume of ion pairs, suggesting that the unit of flow is the ion pair for the moving contact line. Later, the imidazolium-based ILs with identical anion [NTf_2] and different cation alkyl side chain lengths are used as probe liquids for dynamic wetting [127]. Similar conclusion was also drawn where HD cannot be used for the dynamics whereas MKT is relevant in the dynamic process (Fig. 12d). Their results indicated that there is not obvious correlation between the MKT parameters and the size of the ILs. However, the MKT parameters may be susceptible to the water absorption associated with IL at the contact line [127]. Indeed, the presence of water can disorder the contact line no matter whether the ILs are hydrophobic or hydrophilic (Fig. 12e) [130]. Therefore, water absorption from the atmosphere should be taken into account and the careful drying of ILs and inert atmosphere are usually required to perform wetting experiments with ILs [127]. Recently, the spreading dynamics of IL

precursor films has also been studied on a polymer brush surface by a selective dyeing method [131]. The precursor film length of the IL (EMI-TFSI) is identified as the colorless area (Fig. 12f) and the schematic is shown in the lower side of Fig. 12f. The process is divided into two stages (*i.e.*, adiabatic and diffusive stages) for EMI-TFSI, as shown in Fig. 12g. The precursor film elongation length (X) can be described as a power law with respect to time. Specifically, X is expressed as $X \sim t^{0.81}$ in the adiabatic stage (1st stage) and X is increased as $X \sim t^{0.21}$ during the 2nd stage. The authors [131] explained that a large entropy change stemming from strong molecular interaction of EMI-TFSI with polymer brush contributes to the lower advancing velocity of the precursor film for EMI-TFSI than that for the common small-molecule liquid (water).

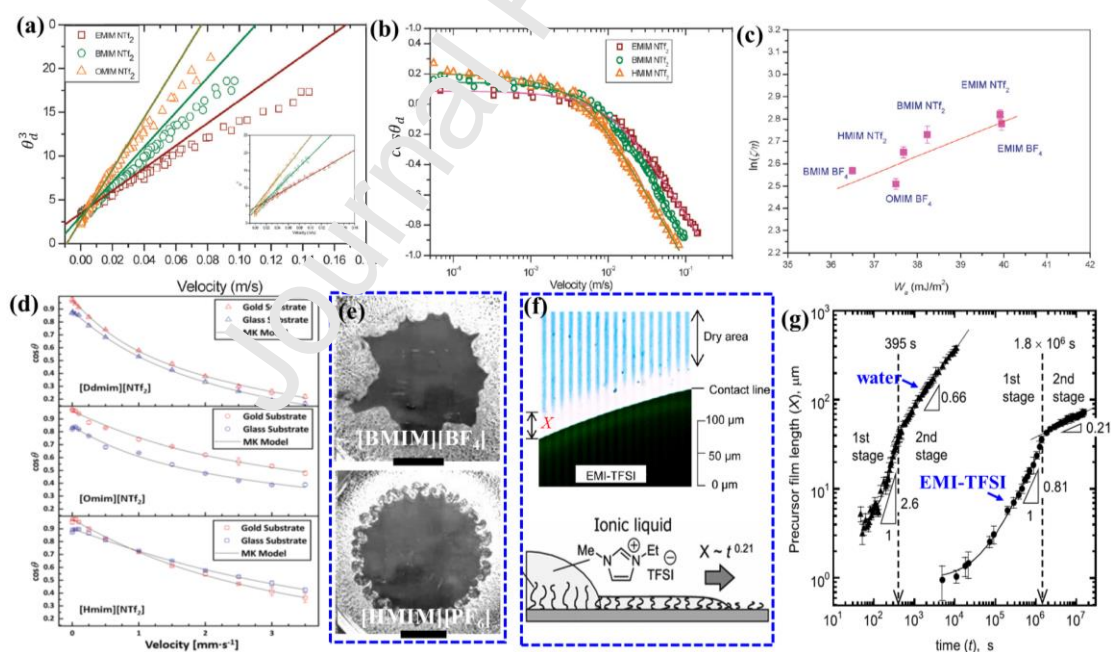


Fig. 12. (a, b) Experimental data for EMIM NTf₂, BMIM NTf₂, OMIM NTf₂, the solid lines are the best (a) HD and (b) MKT fits; (c) $\ln(\zeta/\eta)$ versus W_a for studied ILs. Reproduced with permission [128]. Copyright 2011, Royal Society of Chemistry.

(d) the comparison for $\cos\theta_d$ vs. velocity for ILs on glass and gold substrates, and the solid lines are MKT fits. Reproduced with permission [127]. Copyright 2018, Royal Society of Chemistry. (e) The dispersion state of the mica powder on an aqueous surface, displaying the spreading state for hydrophilic [BMIM][BF₄] and hydrophobic [HMIM][PF₆] with the scale bar of 30 μ m. Reproduced with permission [130]. Copyright 2017, American Chemical Society. (f) Optical image of the precursor film of EMI-TFSI on the line-patterned polymer bush surface. (g) Time evolution of the precursor film for water and EMI-TFSI on the bush surface. Reproduced with permission [131]. Copyright 2011, American Chemical Society.

In addition to the numerous works on wetting dynamics of a liquid in air (so-called “SLG system”) mentioned above, the liquid-liquid displacement on a solid surface (“SLL system”) is also an important subject as it is involved in many technical applications (like enhanced heavy oil production [132]). Besides, this scenario can help us to gain more insight into the initial spreading time because the viscosity of the surrounding liquid can slow down the fast spreading process of the hosted liquid and hence the events at the initial time are precisely captured. Mitra and Mitra [133] reveal that the spreading of the dibutyl phthalate (DBP) and laser-oil droplets surrounded by water always begins in a regime dominated by droplet viscosity with the scaling law of $R_t \sim t$. This initial viscosity-dominated regime gives way to the intermediate inertia-dominated region ($R_t \sim t^{1/2}$) or directly to the ultimate hydrodynamic region (Tanner law, $R_t \sim t^{1/10}$) depending on a characteristic viscous

length scale [133]. They pointed out that the initial viscous regime is a universal nature of the spreading behavior, although it is difficult to be observed due to a lack of adequate spatial clarity and a short time period. The viscous regime and the transition from the viscous to Tanner's regime are further demonstrated by Bazazi et al. [134] who found that the transition time is strongly dependent on the viscosity ratios of the droplet liquid and surrounding liquid. It should be noted that the exponent of the scaling law in the viscous regime may change for the SLL system when surfactants are present in the surrounding liquid, depending on the surfactant types and surfactant contents [98].

The scaling law given above is an empirical approach to quantify the temporal evolution of dynamics for a spreading drop [98]. Given this situation, the MKT and HD models are extensively applied to reveal the mechanism of dynamic wetting for SLL systems in various conditions including solid surface roughness, surface curvature, physio-chemical properties of the surrounding liquid, etc. [97,98,135-138]. Overall, the mechanism of dynamic wetting in SLL systems is thought to be similar to that in SLG systems and the contact line friction in the SLL system may be predicted from the respective single liquid system [139]. Ramiasa et al. [135] suggested that the total contact-line friction in the SLL wetting system is a simple sum of contact line friction of each liquid. This argument is supported by the dynamic wetting model proposed by Seveno et al. [140,141] for the SLL system. Besides, Ramiasa et al. [136] suggested that the motion of the contact line (dodecane/water system) on a nanorough surface is governed by a composite mechanism consisting of the concomitant

adsorption-desorption steps and pinning-depinning events. As shown in Fig. 13a, both solid/liquid surface interactions and surface pinning strength affect the specific activation free energy of wetting controlling the three-phase contact line motion. The effects of solid surface curvature and wettability on the displacement of the contact line are studied by Li et al. [97], who observed a faster oil receding wetting velocity on the hydrophilic surfaces (Fig. 13b) and the role of surface curvature is marginal. The MKT can agree well with the receding data over the low velocity range and does not apply over high velocity range (Fig. 13c). The authors claimed that this is the result of the unreliable measurement at high velocity by their adopted procedure. Analogously, HD can describe the receding dynamics reasonably well in the low velocity regime and fails to capture the data at the high velocity (Fig. 13d). They further point out that the key parameter ζ always increases with the solid surface hydrophobicity and is affected more significantly by the adhesion of the droplets rather than the surrounding liquids to solid surfaces [142]. Besides, the oil receding displacement is affected by the surfactant type (cationic, nonionic and anionic surfactant) [98]. The Marangoni flow and surface hydrophobization arising from the adsorption of surfactant molecules collectively inhibit the oil receding displacement (Fig. 13e). The W_a dependence of $\ln(\zeta/\eta)$ is related to the critical micelle concentrations (CMC) of surfactants (Fig. 13f). It presents a linear dependence of $\ln(\zeta/\eta)$ on W_a at concentrations below the CMC, similar to surfactant-free systems. This linear relation is invalidated at concentrations above the CMC as the thermally-activated jumps may be disturbed by the super-molecular structures of

surfactant micelles near the contact line [98]. Afterwards, the dewetting dynamics of oil is further considered in the surrounding aqueous solution with sodium citrate (Na_3Cit) or calcium ions (Ca^{2+}) (Fig. 13g) [137]. Similar to Li's work [98], the Ca^{2+} inhibits the receding process by increasing the contact line friction due to the enhanced adhesion between oil and solid. Oppositely, the contact line displacement is accelerated by Na_3Cit , arising from the reducing interfacial tension and lower adhesion between oil and solid surface. According to the HD model, the slip length L_s (5~9 orders of magnitude smaller than the molecular size) is not physically reasonable and implies that the HD fails to interpret the dynamics of dewetting oil in their work, despite the clear trend of θ_m and $\ln(L/L_s)$ with the additive ions [137]. Possibly because of this, the authors estimated that the MKT could be more relevant in the SLL wetting system in their recent work [142].

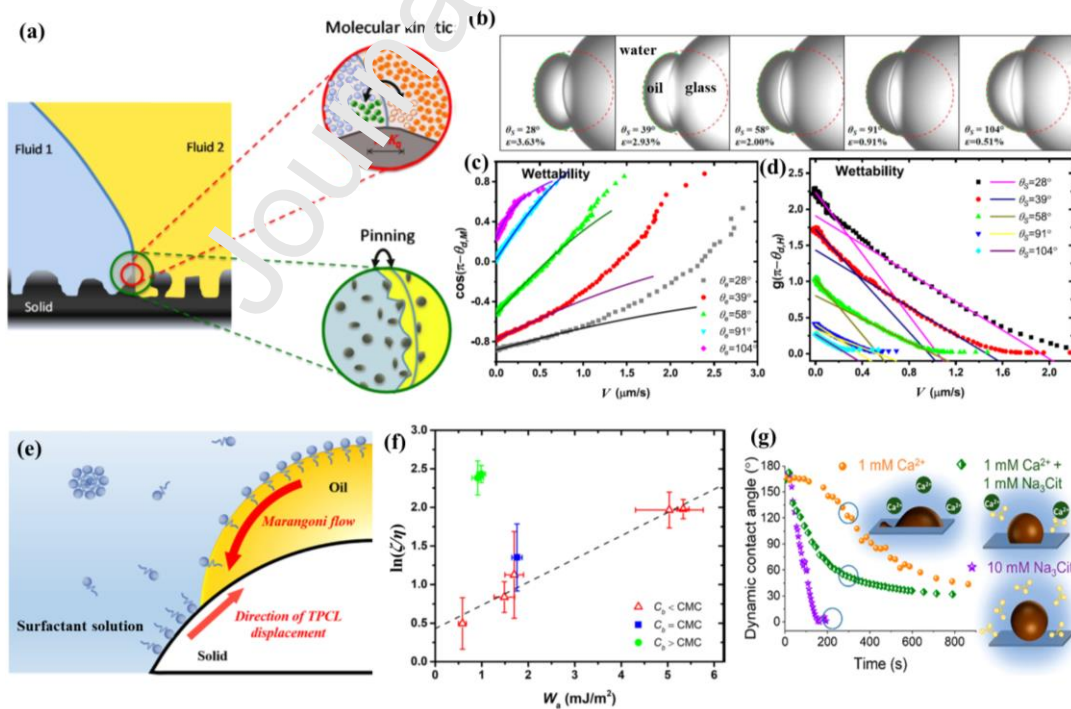


Fig. 13. (a) Scheme of the two mechanisms controlling the contact line motion in the

SLL system. Reproduced with permission [136]. Copyright 2013, American Chemical Society. (b) Snapshots of receding oil droplets on the glass surfaces with variable wettability at maximum deviation factor (ε); (c, d) Cosine functions in MKT (c) and the function in HD (d) for dynamic contact angle vs. the contact line velocity. Reproduced with permission [97]. Copyright 2019, Elsevier. (e) Schematic of the Marangoni flow in the oil droplet arising from the adsorption of surfactants; (f) the plots of $\ln(\zeta/\eta)$ and W_a , and the best MKT linear fit to data points of surfactant concentrations below the CMC. Reproduced with permission [98]. Copyright 2020, American Chemical Society. (g) Schematic of the receding wetting dynamics in the aqueous solution with various ions. Reproduced with permission [137]. Copyright 2020, American Chemical Society.

In addition to surfactant-mediated spreading, another special and interesting case is superspreading that is an anomalously rapid and spontaneous wetting phenomenon typically exemplified by the behavior of trisiloxane surfactant-laden aqueous droplet on a hydrophobic solid substrate [143,144]. There are several factors contributing to superspreading mechanisms including surfactant transfer from the droplet surface to the solid surface, Marangoni flow, formation of surface aggregates, etc., which have been discussed in several recent review papers [145-147]. Concerning the dynamics of superspreading, it is usually characterized by a power law $R_t \sim t^{s_1}$ with R_t the spreading radius or $S_t \sim t^{s_2}$ with S_t the spreading area [146,148]. The exponent s_1 often falls between 0.16 and 1, higher than the exponents of surfactant-free spreading

dynamics (see Table 4), evidencing that spreading has been accelerated. Besides, the increase in surfactant concentration leads to a swift increase of the exponent with a plateau value around 1, which was validated experimentally by Rafai et al. [149]. The substrate surface wettability also affects the superspreading dynamics. For example, Lin et al. [150] reported an exponent $s_2 \sim 1$ on a mango leaf and ~ 0.9 on a more hydrophobic rice leaf. The reason why 2 exponent values were obtained is however not discussed. The dynamics of superspreading is not investigated extensively by now and however, as Kovalchuk and Simmons [146] pointed out, the kinetic studies would contribute greatly to an understanding of the superspreading mechanism.

3.2. Metal liquids

Dynamic wetting of liquid metals and alloys is involved in a wealth of metallurgical processes at high temperature, for example, in soldering, brazing and preparing metal/ceramic composites, etc. The studies focusing on molten metals are usually classified in terms of non-reactive (inert wetting), dissolutive wetting and reactive wetting (chemical wetting) [151-153]. As the name implies, the non-reactive wetting is the process in which a liquid metal spreads on a substrate without dissolution/reaction interaction and typical examples include Pb/Fe, Sn/Mo and Sn/Ge systems [154]; the dissolutive wetting is accompanied by the dissolution of the solid substrate by the spreading liquid, like Sn/Bi, Ag/Cu and Cu/Si systems [153,155]; the reactive wetting is usually the cases where an irreversible chemical reaction occurs and new chemical bonds or intermetallic compounds form at the interface [151,156]. It should be noted that, in a broad sense, dissolutive wetting is also classified into

reactive wetting [152] due to the diffusion of liquid constituents and dissolution of the substrate. The first step is to identify which category the dynamic wetting is, viz., whether the substrate is ideally inert or has solubility or reactivity with the spreading liquids. Then the theoretical analysis can be performed on basis of the approaches already formulated for the room-temperature experiments [151].

The dynamic wetting of non-reactive liquid metals has been a subject of intense research from different aspects, like the metal category, surface roughness, physical field, etc. For Cu, Al, Au and their oxides on Mo substrate, the works of Lopez-Esteban et al. [115,157] exhibited that the spreading velocities are slower than the prediction based on the HD model and implies that the contact line friction dissipation of liquid metals may play a dominate role. This argument was supported by the subsequent molecular dynamics work of Benhassine et al. [158]. Wu et al. [153] compared the effect of substrate roughness on dynamics of non-reactive and reactive wetting by AgCu eutectic alloy/Cu and AgCuTi/Al₂O₃ system respectively. For the non-reactive wetting (AgCu eutectic alloy/Cu system), roughness ($R_a < 900$ nm) can promote spreading whereas reactive wetting (AgCuTi/Al₂O₃ system) exhibits a slower spreading dynamics due to the pinning effect on the rough surface and the formation of interfacial reaction products. Therefore, in their study, the surface roughness exerts an opposite effect on the wetting of inert and reactive systems. In addition to the intrinsic physical properties of liquid/solid systems, the application of an external field is reported to promote the wetting of liquid metals [159,160]. For example, Zhao et al. [160] reported that the ultrasonic field provides an additional periodic force to

destroy the oxide, leading to the decrease of the surface tension of Al melt and facilitating the wetting of Al melt at Al-C interface.

Dissolution of substrates by liquid metals complicates the wetting process since substrates are not perfectly rigid and some other effects (like Marangoni effect, solute-capillary effect, etc.) should be taken into account [151,161-163]. An important and interesting work on dissolutive wetting is the ridge-controlled spreading in the works of Saiz and Tomsia for various metal (Au/Ni, Cu/Ni, etc.) systems (Fig. 14a) [151,162]. Typically, a liquid film (100 ~ 400 nm) ahead of a macroscopic Au drop can be observed on a Ni substrate and the continuous film consists of Au and Ni, implying a high degree of mutual solubility for Au and Ni components. During the simultaneous spreading and dissolution of the Au/Ni system, the compositional variation at interface can result in surface tension gradients ($d\gamma/dx$) driving the formation of Marangoni films (see schematic in Fig. 14a). The surface tension at the edge of the film is higher than that at other positions of the film due to the compositional variation and a triple line ridge is formed at the film edge. The ridge can pin the wetting liquid front and cause a stick-slip motion. Therefore, the wetting velocity and dissolution rate should be carefully compared and the influence of interfacial dissolution and the possible ridge formation on dynamic wetting are separately quantified. It is demonstrated that the dissolution does not have a significant effect on an Au/Ni wetting system whereas an opposite conclusion is drawn for a Cu/Nb system [162]. Saiz and Tomsia [151] further compared the wetting dynamics of metal systems to MKT and HD model. It suggests that the main channel

of dissipation is the contact line friction rather than the viscous dissipation (Fig. 14b) for the metal systems. However, different views on dissolutive wetting were recently reported by Sun et al. [164] for the Cu/TC4 titanium alloy and Cu/304 stainless steel (304ss) systems. According to the binary phase diagrams of the Cu/Ti and Cu/Fe systems, Cu/TC4 and Cu/304ss systems exhibit typical dissolutive wetting without new compound formation, as validated by SEM and EDS analysis (Fig. 14c and d). The authors suggested that the drop spreading is diffusive transport dominated for both systems, rather than thermo-capillary and solute-capillary controlled based on the analysis of heat distribution, the presence of a uniform solute at the contact line, and the calculation of Peclet, Reynolds, and capillary dimensionless numbers. Their interpretations of the underlying mechanisms are derived from the $R_f \sim t^{m_2}$ scale law. As shown in Fig. 14e, the slope m_2 is close to 1/4, *i.e.*, evidencing diffusion limited wetting [161]; the values of m_2 for the Cu/304ss system (Fig. 14f) fall into the range of 1/10 (HD model) and 1/4 (diffusion-limited reactive wetting). This implies that the contact line friction may not be the main channel of dissipation channels for both Cu/TC4 and Cu/304ss systems on basis of the authors' analysis [164].

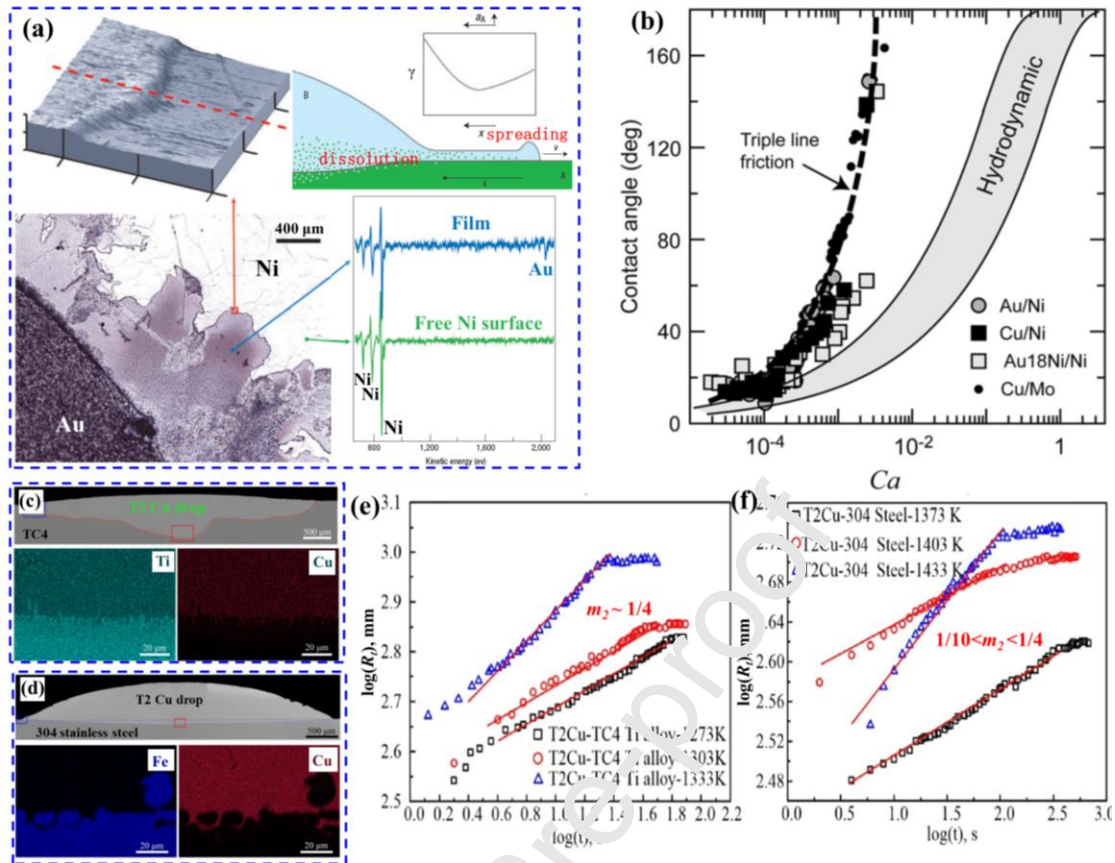


Fig. 14. (a) AFM and optical images of Au/Ni system, schematic for the formation of a Marangoni film and ridge in the system with mutual solubility and Auger electron microscopy spectra for the film. Reproduced with permission [162]. Copyright 2004, Springer Nature. (b) Spreading dynamics of metal systems with various solubility. Reproduced with permission [151] Copyright 2005, Elsevier. (c, d) SEM and EDS images of (c) T2Cu/TC4 system and (d) T2 Cu/304ss system after isothermal wetting; (e, f) Plots of $\log(R_t)$ vs $\log(t)$ for Cu spreading on (e) TC4 and (f) 304ss substrates. Reproduced with permission [164]. Copyright 2019, Elsevier.

Reactive wetting of liquid metals is a very intricate process possibly simultaneously involving diffusion, chemical reactions and convection, and, however, is key to multiple metallurgical processes for which a good wettability of liquid

metals with the substrate guarantees the excellent properties of the final products [165-167]. Yet, the wetting community seems unable to find common ground on the issue of whether interfacial reactions promote or restrain wetting [151,165,167,168]. Some researchers supposed that the reactivity enhances wetting as verified by a better wettability of the interfacial products [166,169] or postulated by decreasing interfacial energy [170]. On the contrary, the multiple evidences [165,168,171] indicate this is not necessary because (i) the interfacial intermetallic compounds may not cover the whole interface (in most cases, the interfacial reaction product is formed at the initial contact region) and (ii) spreading velocity is much faster than the interfacial reaction and the reaction cannot exert influence on wetting dynamics even if interfacial reaction product changes the wettability. Herein, the wetting dynamic of liquid Al melts/solid is taken as an exemplary system to simply illustrate this debate due to the wide application and easy formation of the Al-rich intermetallic compounds. Sun et al. [166] found that the intermetallic compound formation removes the oxide film present on the Ni substrate and the energy liberated at the interface increases the wetting driving force, eventually accelerating the spreading of liquid Al. A similar result on the interfacial reaction-controlled wetting dynamics was also supported by Shi et al. [167]. Inversely, Ramos-Masana and Colominas [168] suggested that spreading dynamics of liquid Al on a coated steel substrate with reactive reaction is significantly lower than that on the bare steel substrate. Concerning the mechanism of reactive wetting, the channels of energy dissipation are seldom discussed by the classical wetting dynamics models [91], in which the energy variations induced by the

interfacial reactions are not taken in account. Instead, the reaction limited model (or called “reaction product control model”) suggested by Dezellus and Eustathopoulos et al. [169,172,173] is usually used to discuss the effect of interfacial reactions on reactive wetting. However, the work on the modelling of reaction limited model is beyond the scope of this review as it has been presented in other reviews [172,173].

3.3. Polymer liquids

The pioneering drop spreading experiments of polymer melts were performed in the late 1960s [174-176] and some rudimentary concepts and frameworks were discussed. These studies may have inspired the subsequent works of Blake [53] and Voinov [52], originators of the main dynamic wetting theories. Then, in the de Gennes’ seminal review paper [10], the question of the spreading of polymer melts was already raised with the possible existence of a "protruding foot" surrounding the polymer cap. The later cornerstone review by Bonn et al. [39] also identified the spreading of polymers as a hot and important topic. Yet, since then, very sporadic studies have tried to shed more lights on this topic, possibly due to the intrinsic complexity of polymer melts (dispersity, non-Newtonian behavior and strong slip at interface) [177]. For example, Chiappori et al. [178] studied the wetting of molten Nylon-6 drops on silica, Rwei and Su [179] measured contact angle relaxations of polystyrene (PS), Poly(methyl methacrylate) (PMMA), and Poly(trimethylene terephthalate) (PTT) on a TiO₂ substrate, and Bex et al. [180] studied dynamic spreading of polypropylene (PP), polyethylene (PE) and polycarbonate (PC) melts on

thermoset substrates. These studies improved the basic understanding of the wetting dynamics of molten polymers *via* the interaction between the polymers and the substrates, but they did not elaborate on the different channels of energy dissipation driving the dynamics. Therefore, in this respect, the wetting dynamics of molten polymers is less common in comparison to small-molecule and metallic counterparts.

Zhang et al. [92] first challenged the available dynamic wetting theories against the spreading dynamics of molten PP and poly(vinylidene fluoride) (PVDF) drops (Fig. 15a) with a motivation to check the suitability of the classical models and identify the dominating channels of energy dissipation. Due to their high viscosity, the spreading dynamics of the molten polymer systems are well modelled by the HD model (Fig. 15b). Surprisingly, the MKT is also able to describe the experimental data (Fig. 15c), obscuring the role of the energy dissipation channels. It was also hypothesized that the jump length gives a good estimation of the Kuhn segment length, a key property of polymer chains, with the extra benefit of avoiding the use of relatively uncommon large-scale equipment, like small-angle neutron scattering (SANS), etc. [181]. It would be an important step if the dynamic wetting theory and the statistical theory of polymer chains were successfully combined. Subsequently, Soleymaniha and Felts [104] developed the tapping mode AFM technique to monitor the spreading dynamics of molten PS droplets at the nanometer scale (Fig. 15d). They compared the dynamics to the MKT, HD and de Ruijter combined model and found all the three models are compatible in the spreading with acceptable accuracy (Fig. 15e and f). The authors argued that spreading dynamics is dominated by the viscous

dissipation mechanism (occupying roughly 75% of the total dissipation) according to the de Ruijter combined model, but the way to draw the conclusion of the ratio and its validity are highly debatable since the de Ruijter combined model is not able to judge the specific ratio of viscous and frictional dissipations [59].

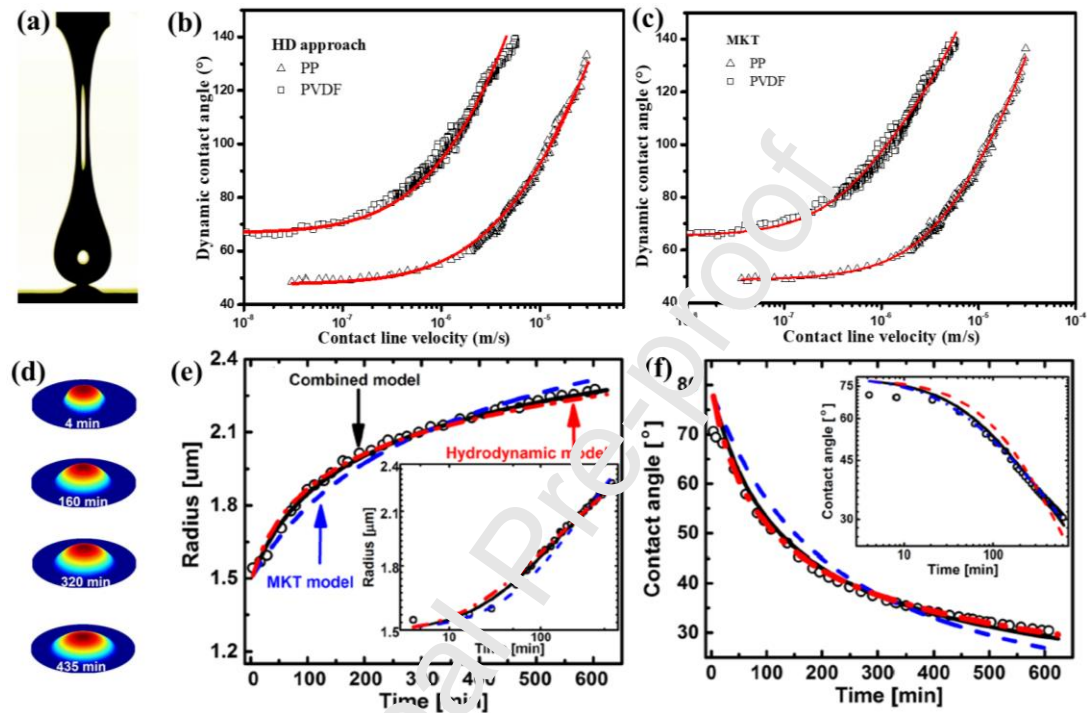


Fig. 15. (a) The optical image of a molten PP drop at the contacting time; (b, c) the contact line velocity dependence of dynamic contact angle fitted by the (b) HD and (c) MKT models. Reproduced with permission [92]. Copyright 2017, American Chemical Society. (d) the 3D profile of a spreading PS droplet over time; (e, f) The fits of HD, MKT and de Ruijter combined model to (e) dynamic radius and (f) dynamic contact angle. Reproduced with permission [104]. Copyright 2018, American Institute of Physics.

Several important research works have endeavored to address the issue of the

ambiguity of the dominant channel(s) of energy dissipation by illustrating the influence of the molecular weight dispersity on the wetting dynamics of polymer systems. The wetting behaviors of molten polymers are then often modelled by polydimethylsiloxane (PDMS) liquids as they can show a narrow dispersity and a wide range of tailored viscosities with almost unchanged surface tensions, which offers an opportunity to clarify the viscosity (likewise, the molecular weight) dependence of the dissipation channels for polymers [16,103,105,182]. Indeed, Vega et al. [16] experimentally distinguished the MKT and HD regimes (i.e., frictional and viscous dissipations) in the capillary rise of PDMS liquids on a vertical fiber by selecting a series of PDMS liquids with various viscosities. Typically, the PDMS5 and PDMS500 (PDMS liquids with kinematic viscosities of 5 and 500 mm²/s) follows the MKT behavior and HD behavior, respectively. Zhang et al. [100] further studied the viscosity dependence of PDMS5/PDMS500 mixtures (Fig. 16a) and found that the MKT/HD transition moved to a higher viscosity regime for the PDMS mixtures (transition viscosity: 27.4 ~ 32.8 mm²/s) compared to single PDMS liquids (transition viscosity: 10 ~ 20 mm²/s) (Fig. 16b). It is proposed that the segregation of shorter chains at the liquid/air interface is responsible for the change of the MKT/HD transition (Fig. 16c). That is to say, PDMS5 chains with smaller sizes concentrate in the vicinity of the liquid/air interface to a larger extent than in the bulk, leading to a lower local viscosity that determines the dominant channel of energy dissipation. The mobility of short and long chains is compared and illustrated by the diffusion constant (D) in the work of Peters et al. [183]. D_s (D for the shortest 5% of the chains) deviates

more considerably from D_a (averaged D over all chains) than does D_L (D for the longest 5% of the chains) in Fig. 16d, indicating that the short chains move significantly faster than the long chains. Moreover, the short chains can promote the motion of the long chains in the dispersed melt as the increased diffusion of the shorter chains leads to constraint release for the longer chains [183]. This offers an important evidence for the surface segregation of short chains during dynamic wetting. The argument is also supported by other works [184,185]. For example, Yao et al. [184] found a similar result on capillary imbibition of poly(ethylene oxide) (PEO) mixtures in nanopores. The nanopores are enriched on average by $\sim 15\%$ of the shorter PEO chains (sketched in the inset of Fig. 16e). This enrichment is verified *via* gel permeation chromatography (GPC) experiments of PEO mixtures present in the bulk and in the pore interior (Fig. 16e). Actually, several physical factors (such as miscibility, elasticity/rigidity, etc [17,183,186]) of polymer mixtures can contribute to the surface segregation of short chains. This is dictated by the thermodynamics of the systems characterized by the parameter χN (χ is the miscibility parameter of the two components in the polymer mixture and N is the molecular weight of the migrant). As sketched in Fig. 16f, a high concentration (ϕ_1) of the migrant small molecules (black short chain) is reached at the interface and a thick wetting migrant layer can be obtained with increasing χN . The calculations of the Schmidt-Binder mean field theory and self-consistent field theory suggest that the fraction of the migrant short chains on the surface is significantly inhibited as the elastic modulus (\tilde{B}) of the polymer increases (see $\phi(z)$ curves in the main panel of Fig. 16g with elasticity and

the inset of Fig. 16g without elasticity) [47]. In parallel to the molecular size (or molecular weight) of polymer components, the difference of surface tension can also lead to the surface segregation effect as the polymer component with the lower surface energy will segregate to the interface, as revealed by several authors [185,187-189]. In terms of molten polymers, surface segregation driven by the difference in the molecular size rather than surface tension seems to help further deepen the understanding the wetting dynamics due to the intrinsic dispersed molecular weight distribution. However, there are several open questions for surface segregation of short chains, such as the time dependence of surface segregation, the influence of dispersity and reptation of the polymer chains on surface segregation, the real local viscosity in the vicinity of the contact line and its effect on the dominant energy dissipation channel, just to name a few. In this respect, molecular dynamics simulations [190] may be an alternative methodology to unravel these questions.

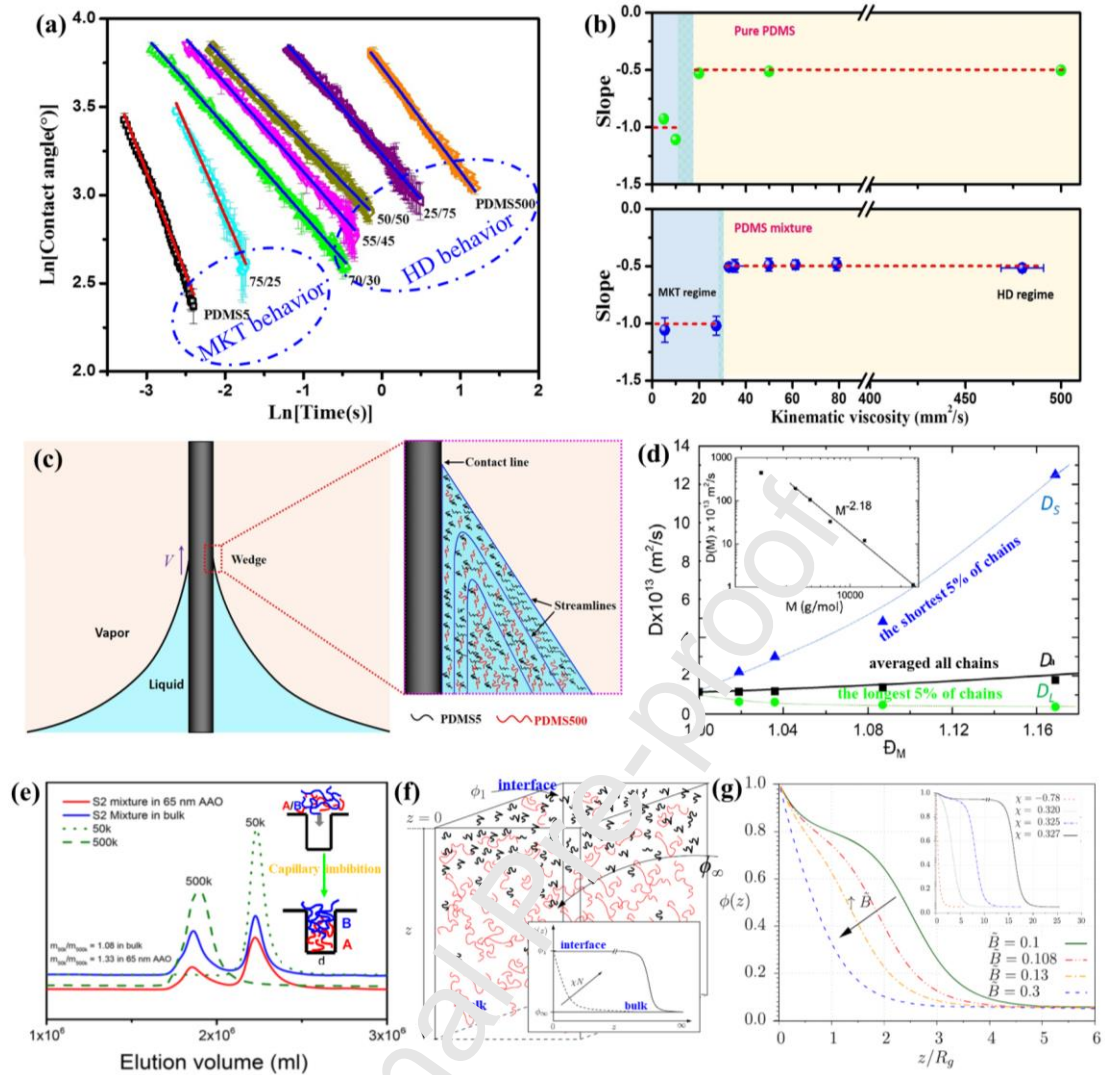


Fig. 16. (a) Contact angle dynamics vs time for PDMS5, PDMS500 and their mixtures with different ratios. (b) Slope of $\ln \theta_d$ vs $\ln t$ in one-component PDMS liquids and two-component PDMS mixtures. (c) Schematic for the capillary rise in the vicinity of the contact line for a two-component PDMS mixture. Reproduced with permission [100]. Copyright 2018, Elsevier. (d) Diffusion constant D vs the dispersity D_M . Reproduced with permission [183]. Copyright 2013, American Physical Society. (e) GPC traces of PEO 50k (molecular weight), PEO 500k (molecular weight), S2 (PEO 50k/PEO 500k = 50/50) mixture in the nanopores (diameter: 65 nm) and in the bulk. Reproduced with permission [184]. Copyright 2018, American Chemical Society. (f) Schematic for a mixture of low (black) and high (red) molecular weight polymers

(main panel) where migrant concentration profiles for different χN values with the concentration in bulk ($z \rightarrow \infty$) and at interface ($z=0$) are denoted by ϕ_∞ and ϕ_1 (inset). (g) Migrant concentration profiles $\phi(z)$ with elasticity (main panel) and without elasticity (inset). Reproduced with permission [47]. Copyright 2016, American Physical Society.

3.4. Simulated liquids

Molecular dynamics (MD) is a powerful technique to access the details of wetting at the molecular level by solving the classical Newtonian motion equation. It enables us to tailor individual parameters separately with great precision in a way that is nearly impossible in a real experiment. For instance, the solid/liquid interaction can be systematically varied independently of quantities like viscosity, density and surface tension. The results of MD simulations can be compared to experiments, allowing to verify the validity of assumptions supporting theoretical models or even discover new physical phenomena that are not observable experimentally. On the negative side, the number of atoms (typically $\sim 10^6$) in practical simulations is very small compared to those (typically $\sim 10^{23}$) in a real experiment [41]. However, such limitation does not prevent us from simulating realistic experiments and useful macroscopic properties can be deduced from MD simulations. The main components to simulate the dynamic wetting contain the liquid, the substrate, and their interaction. Lennard-Jones (L-J) liquid molecules are typically linear chains with a few atoms (2 ~ 64 atoms). The viscosity and the surface tension can be controlled by the length of the chains. The solid/liquid interaction, *i.e.*, the solid/liquid affinity, is modelled by the standard

pairwise Lennard-Jones (L-J) interaction, which is expressed as

$$U(r_{ij}) = 4C_{A-B}\epsilon_{ij} \left[\left(\frac{\sigma_{ij}}{r_{ij}} \right)^{12} - \left(\frac{\sigma_{ij}}{r_{ij}} \right)^6 \right] \quad (24)$$

where r_{ij} is the distance for the given pair of atoms i and j , the relative affinity is controlled by the coupling parameter C_{A-B} where the subscript $A-B$ means the possible interaction pairs of L-L, L-S and S-S, the parameters ϵ_{ij} and σ_{ij} are the depth of the potential well and the effective atomic diameter. The C_{A-B} is fixed to 1 for the L-L and S-S couplings in a simplified simulation, and C_{A-B} for L-S coupling is tailored to specify the solid/liquid affinity that determines the equilibrium contact angle. A large equilibrium contact angle is expected if the L-S coupling is smaller than 1, and vice versa.

Since the pioneering MD studies of Koplik et al. [191] and Thompson et al. [192], many MD works have been performed to investigate the mechanisms of dynamic wetting from different aspects. They include the spontaneous wetting (like spreading of drops on flat surfaces, capillary rise around fibers or liquid rise in capillaries) and forced wetting (like forced wetting of fibers) [193,194]. These works have confirmed that the wetting behaviors and the physical variables of the simulated systems can closely reflect the real experiments. For example, Bekele et al. [193] examined the spreading dynamics of water nano-droplets on a completely wetting surface and the scaling law for the base radius evolution is well described by the HD model for low contact angles. MD simulation results are also compared with the experimental results of Kim et al. [195] and a good agreement is found. Additionally,

their MD simulations [193] illuminate a missing finding in experiment that is the unified temporal variation of droplet height.

At the macroscale, a liquid drop in mechanical equilibrium seems static. In contrast, at the nanoscale, due to the existence of thermal fluctuations, dynamic equilibrium processes dominate. It also holds for the contact line where the liquid molecules constantly fluctuate with a certain configuration and position. Recently, Fernández-Toledano et al. [48,196,197] performed a series of MD simulations to model the contact line fluctuations for improving the understanding of dynamic wetting at the molecular level. They first focused on the fluctuations of the contact lines of a liquid bridge at equilibrium between two solid surfaces (Fig. 17a) [48]. The mean locations of the contact line fluctuations with a Gaussian distribution (Fig. 17b) are modelled by overdamped one-dimensional Langevin harmonic oscillator, from which the ζ is extracted. Another ζ_{MKT} is independently obtained by performing a drop spreading MD simulations applying the MKT. The comparison of these obtained coefficients revealed an excellent agreement as a function of the solid-liquid coupling C_{SL} (Fig. 17c). Based on this, the velocity-dependence of dynamic θ_m can be calculated and predicted at different solid-liquid couplings (Fig. 17d). It suggests that the dynamic wetting could be predicted by studying the fluctuations of the contact line at equilibrium. The authors [105] extended this approach to a moving contact line with thermal fluctuations (Fig. 17e). Similarly, the mean location of a moving contact line fluctuations can be interpreted in terms of a Langevin formalism analogous to that at equilibrium. The MD simulation results show that the plate velocity (U_{plate})

does not affect the values of ζ within the error bars (Fig. 17f). Besides, almost identical values of ζ can be obtained for the drop spreading simulation, the thermal fluctuations of the contact line at equilibrium and the fluctuations of the moving contact line (Fig. 17g) at different C_{SL} values. It indicates that the fluctuations, irrespective of whether the contact line is moving or not, contains the necessary information to predict the dynamic wetting. Their further work suggests that the measurement of the contact-line fluctuations of a water-like liquid may also predict slip by establishing the link of the contact line friction and the coefficient of slip [197]. Since the contact line fluctuations are ubiquitous, the contact line friction is an intrinsic wetting phenomenon and hence the theoretical approaches of dynamic wetting ignoring the contact line friction are supposed to be incomplete.

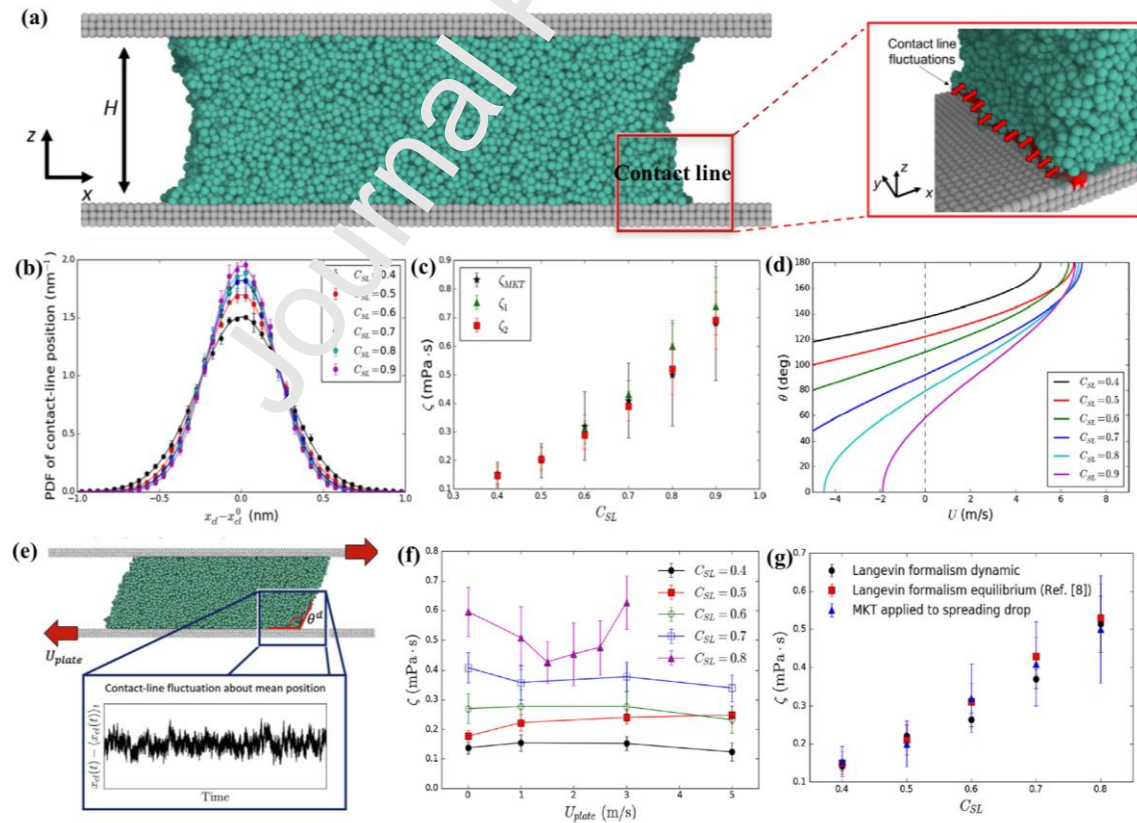


Fig. 17. (a) Snapshot of the liquid bridge between two solid plates at equilibrium; (b)

Probability density function (PDF) of the mean locations for the contact line position and their Gaussian fits. (c) the relation between ζ and C_{SL} ; ζ_1 and ζ_2 are values from two methods of the contact line fluctuations, ζ_{MKT} was independently obtained by a spreading drop simulation. (d) The predicted velocity dependence of θ_m at different solid-liquid couplings. Reproduced with permission [48]. Copyright 2019, Elsevier. (e) Snapshot of the liquid bridge between two solid plates with the moving plate velocity (U_{plate}) in opposite directions. (f) Contact line friction ζ versus U_{plate} at each solid-liquid coupling. (g) The comparison of ζ values from the thermal fluctuations of moving or equilibrium contact line, and drop spreading. Reproduced with permission [196]. Copyright 2020, Elsevier.

4. Applications

The fundamental insights described above provide great opportunity to develop diverse products for the industry or our daily life, leading to an accumulation of new applications [198,199]. We mainly present the emerging applications related to wetting, such as the manipulation of flow liquid, water harvesting, printing, etc. in this section.

4.1. Manipulation of flow behavior

Liquid flows are often observed in daily life, like the tea flow poured from the tea spout (so called "teapot effect") and walking or car-driving on a wet ground after raining, where the solid/liquid separation is interpreted in terms of the flowing bending of stream lines. Duez et al. [200] demonstrated that the wetting property has a

key influence on the flow pattern. The flow liquid film can be tuned and ejected from the superhydrophobic substrate, hereby avoiding liquid trickling along the solid surface [200]. Later, Dong et al. [201] carried out a detailed and practical work on the liquid flow that is affected by wetting. The liquids show similar behaviors (complete overflow, separation, and overflow with splashing) on the hydrophilic and hydrophobic surfaces (Fig. 18a and b, upper). A superhydrophilic or superhydrophobic surface can be achieved by micro/nanostructured polymer coatings. It is found that the liquid overflow is enhanced by superhydrophilicity whereas it is substantially reduced by superhydrophobicity (Fig. 18a and b, lower). There is a Coanda effect that is pull-back behavior due to the pressure drop (ΔP) across the liquid film [202]. The capillary-adhesive force (F_{ca}) and Coanda effect together plays the role of a centripetal force, facilitating the overflow behavior on the superhydrophilic surface (Fig. 18c, upper). Inversely, air entrapment into micro/nanostructures prevents the fluid from contacting the superhydrophobic surface and counteracts the pressure difference (so-called Coanda effect) on the flowing liquid, leading to a horizontal parabolic flow with long velocity range (Fig. 18c, lower). These results indicate that the flow behavior of liquids can be manipulated by the wetting properties of solid surface due to the strong capillary effect at low velocity and large Coanda effect at high velocity, which has obvious practical implications. For example, the authors prepared a tire with different wetting properties on two sides where superhydrophilic polymer coating is treated on one side and the other side is untreated *i.e.* hydrophilic. Nearly no splashing is observed on the superhydrophilic

sidewall whereas an apparent splashing is produced by the hydrophilic sidewall (Fig. 18d). Besides, another practical example is the commercial shoe modified with a superhydrophobic polymer coating. The walking test of the modified shoe was conducted by walking on a muddy land. The untreated shoe has significantly suffered with muddy wetting and no such wetting phenomenon is observed on modified one (Fig. 18e). It suggests that the interfacial interaction between the dynamic liquid and solid surface can be manipulated to control the liquid flowing behavior.

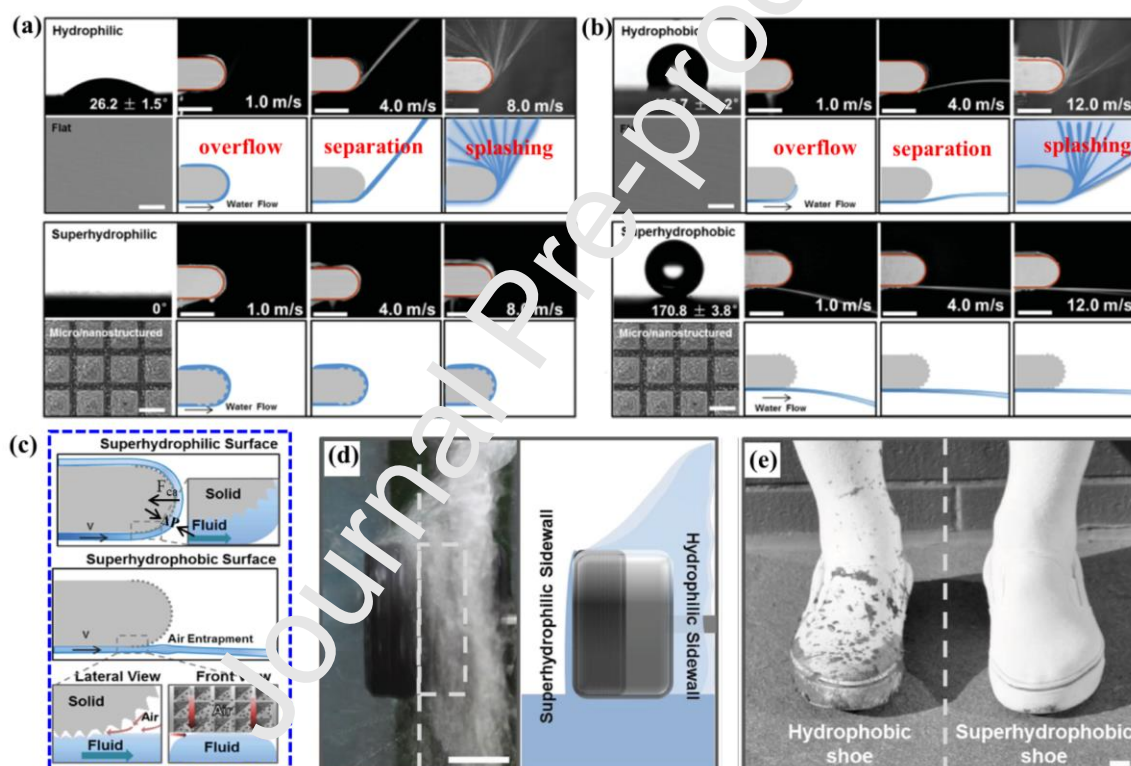


Fig. 18. (a, b) Water contact angle and SEM images of the plates (left), optical images and corresponding schematic of liquid flow behaviors (right), scale bars: 5.0 mm. (c) the schematic for the details on the solid/liquid interface. (d) Optical images and corresponding schematic for flow dynamics on the tire, scale bars are all 2.0 cm. (e) Comparison of the muddy wetting on the shoes with and without treatment, scale bars: 2.0 cm. Reproduced with permission from [201], Copyright 2015, Wiley-VCH.

4.2. Water Harvesting

Directly harvesting water is an alternative approach to collect drinking water from the atmosphere and solves the water shortage issue. Inspired by nature (Namib desert beetle [3], spider silk [4], *Cotula fallax* plant [203], etc.), numerous researchers attempted to prepare and optimize nature-inspired materials with superhydrophobic and superhydrophilic surface characteristics that facilitate atmospheric water capture [6,204-207]. Among them, Neto and co-workers [208-210] highlighted the role of dynamic wetting for optimizing water capture. They [208-210] created micro-/nano-patterned surfaces consisting of hydrophilic poly(4-vinylpyridine) (P4VP) patterns on a hydrophobic PS background by the spontaneous dewetting of polymer bilayers. Typically, the dewetting of the P4VP film from a PS film produces micro-/nanoscale P4VP patterns (Fig. 19a) triggered by the initial film thickness change and annealing procedure. The resulting topography mimics the Namib desert beetle exoskeleton. The authors [208] pointed out that the motion of the contact line (Fig. 19b) on the patterned surfaces is crucial to the optimization of surface coatings for atmospheric water harvesting. Similar to forced wetting, the dynamic receding contact angle reduces with the increase of the withdrawing velocity (Fig. 19c). The authors claimed that, in such case, the contact line friction dominates the energy dissipation over viscous dissipation (the MKT fitting curves are not shown in Fig. 19c). Besides, the HD approach can fit well the wetting dynamics in the high Ca regime (Fig. 19d) and a deviation from HD approach is observed at low Ca regime for

the three surfaces. The most pronounced deviation is found for the micropatterned surfaces, as the P4VP bumps with large sizes create obvious jumps in the surface wettability and pinning effect, which is useful for evaluating the performance of the patterned surfaces as platforms for harvesting atmospheric water [208]. For example, the patterned surfaces were evaluated to capture water relative to the hydrophilic P4VP surface (Fig. 19e and f) [209]. The nucleating and growing of water droplets are irregular in shape on hydrophilic P4VP surface (Fig. 19e), and eventually water films are formed. Under such circumstances, the surface is thermally insulated from the humid air and the water condensation is slowed down, and therefore, the film-wise condensation is detrimental for water capture [211]. By contrast, water condensation preferentially happens on the hydrophobic patterns (Fig. 19f). The adjacent droplets become large enough and span the PS region, leading to the formation of coalescence [209]. They also quantitatively compared the ability of micropatterned surfaces to capture atmospheric water relative to PS and P4VP film [210]. The volume of condensed water per unit surface area on the P4VP-patterned surface shows approximately 45% and 82% enhancement than that on the P4VP film and PS film, respectively (Fig. 19g). Besides, the significant enhancement in the rate of condensation can be obtained on the patterned surface compared with P4VP and PS films (Fig. 19h). Specifically, it can reach $3.4 \pm 0.2 \text{ L m}^{-2} \text{ h}^{-1}$ under conditions of high flow rate (corresponding to a realistic wind speed of approximately 10 km h^{-1}) for the micropatterned surface. In addition, the authors found that the micropatterned surface promotes the easier detachment of water droplets in comparison with the hydrophilic

P4VP films. The critical detachment droplet volume ($12.7 \mu\text{L}$), which is predicted by Furmidge's equation involving the dynamic contact angle [210], for the micropatterned surface is smaller than that ($29.9 \mu\text{L}$) of P4VP film. These results demonstrate that it is possible to harvest a significant amount of water by the patterned surfaces directly from the atmosphere.

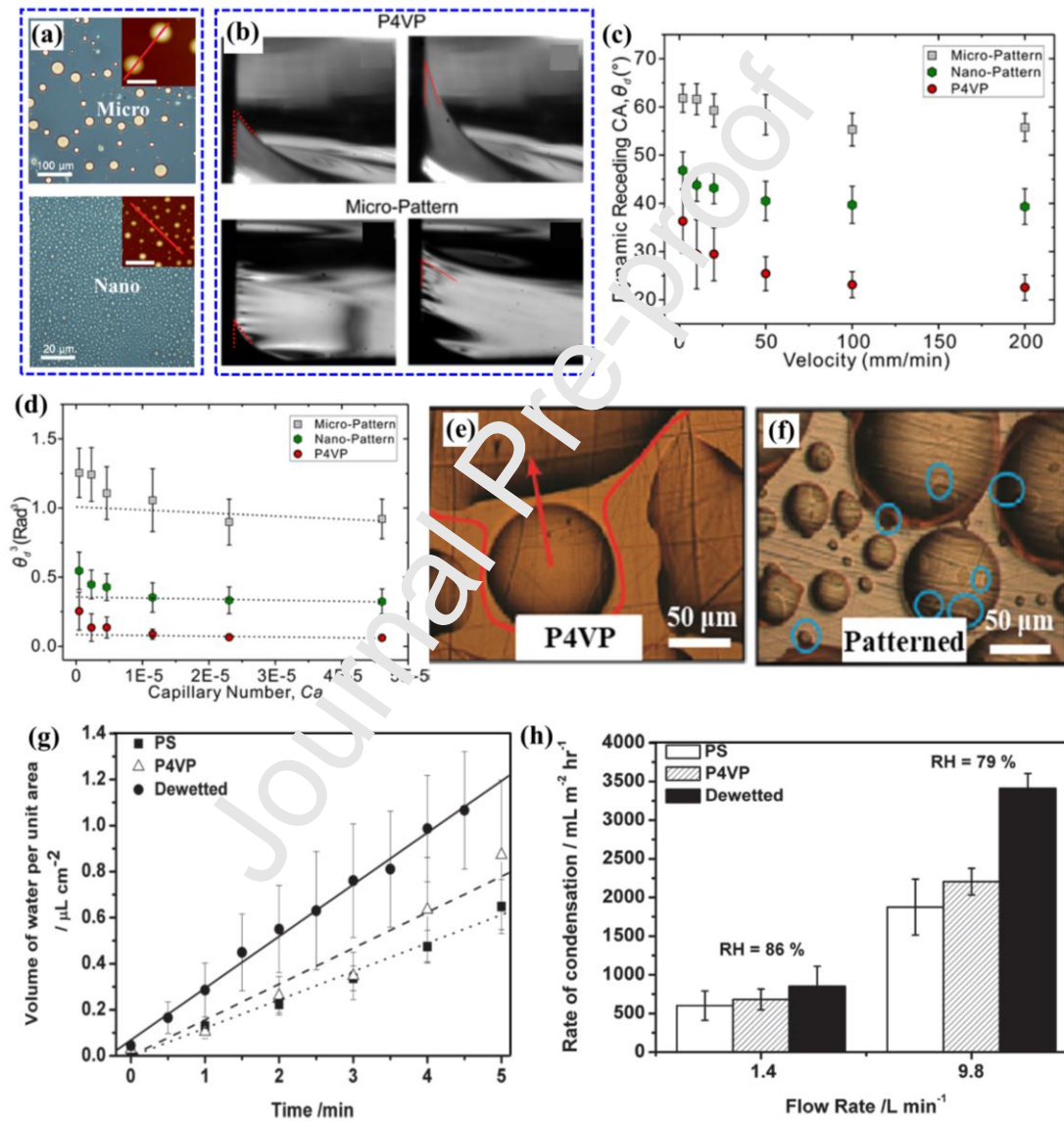


Fig. 19. (a) Optical and AFM (inset) images of the P4VP/PS dewetted bilayers with nano/micro patterns. (b) Side-view optical images of the capillary rise against the P4VP and micro pattern substrates at static state (left) and dynamic equilibrium with a

withdrawn velocity of 200 mm/min. (c) Dynamic receding contact angles versus withdrawing velocity for the three surfaces. (d) the cubic dynamic receding contact angles versus capillary number for the three surfaces. Reproduced with permission [208]. Copyright 2017, American Physical Society. (e, f) Optical images of water condensation at the dew point on the (e) P4VP film and (f) P4VP-patterned PS film, in which the P4VP patterns are highlighted in blue lines and the droplets encircled in red lines. Reproduced with permission [209]. Copyright 2017, American Chemical Society. (g) Volume of water per unit area vs. the time in a time-lapse microscopy (relative humidity (RH): 60%). (h) Rate of condensation ($\text{mL m}^{-2} \text{h}^{-1}$) on the sample surfaces under a flow of humidified air. Reproduced with permission [210]. Copyright 2011, Wiley-VCH.

4.3. Printing

Printing is a key type of information communication and expression and has been involved into many aspects of our life, like publishing, packaging and integrated-circuit packaging in the electronics industry, etc. [212]. Remarkable progresses have been achieved towards the high-resolution, flexible, eco-friendly, low-cost, addressable and scalable printing technique in the recent decades. In most techniques, the drop is employed as a transfer carrier containing some nanoparticles or some other colored elements. Then the liquid carrier evaporates and hence the solute is patterned on the surface for a specific requirement. The drop shape will change with time depending on the wetting properties (such as surface tension) of the

drop, the impact speed of the drop as well as wettability of the plate (or substrate) surface [212-215]. That is where spreading dynamics of the contact line plays a role in the printing process. The corresponding droplet spreading is usually directed to pattern the substrate by locally varying surface topology or surface tension. For example, Léopoldès et al. [216,217] reported the wetting behavior of droplets jetting onto surfaces patterned with lyophobic and lyophilic stripes. The final droplet shape hinges on the drop size relative to the stripe width. When the drop moves in the region with a different wettability, the dynamics of moving liquid is determined by the relation between driving force and the variation in surface force. The authors underlined the inherent difficulty in controlling the formed pattern details using inkjet-printing due to the subtle effect of the surface properties of the patterned substrates on the liquid wetting behavior [216].

Besides, Lim et al. [218] demonstrated that the contact line dynamics and the evaporation behavior of the moving drop may be the key elements for inkjet printing. The wetting and drying behaviors of inkjet-printed organic semiconductors, *i.e.*, 6,13-bis(triisopropylsilylethynyl) pentacene (TIPS_PEN) are deposited on a dielectric surface with controlled surface wettability using various self-assembled monolayers (SAMs). On the hydrophilic surface, the drop first spreads towards equilibrium (Stage I) and then recedes until the contact line is pinned (Stage II) (Fig. 20a). At Stage III, the nucleation of TIPS_PEN preferentially occurs near the contact line due to the outward hydrodynamic flows stemming from the contact line pinning (Fig. 20b). Finally, the inkjet-printed TIPS_PEN crystals with ordered crystalline structure are

formed on hydrophilic surfaces (Fig. 20c). By contrast, it shows different wetting and drying stages on the hydrophobic surface (Fig. 20d). It is found that no outward hydrodynamic flows are triggered around the contact line, and the TIPS_PEN molecules with random orientation of crystals are formed due to the continuous receding without contact line pinning. The results suggest that the control of the contact line and evaporation dynamics of the carrier drop play an important role in printing the organic semiconductor films with a tailored molecular orientation, which helps to address the major challenge of direct-write fabrication of high-performance organic devices [219]. Recently, Fernández-Torredano et al. [215] have made an important progress in the relation between drop wetting, impacting and nanoprinting using large scale MD simulations. A typical snapshots of the impacting drop is shown in upper side of Fig. 20e. The lower side of Fig. 20e suggests that a critical impact velocity exists at which the drop contact diameter (D_{eq}) never exceeds the equilibrium value that is dependent on the substrate wettability. A new model for the maximal contact diameter (D_{max}) is proposed with the consideration of the roles of the impact velocity and wettability [215], which has the ability to successfully predict the D_{max} based on the initial diameter D_0 for any impact and wettability. With the model and the scaling law for the time t_{max} to reach D_{max} ($t_{max} \propto We^{-1/5}$), a master curve collapsing temporal evolution of the base diameter $D(t)$ is presented before reaching D_{max} (Fig. 20f). The results suggest that nanoprinting becomes predictable and it helps design a better nanoprinter to achieve a smooth and homogenous coverage of the surfaces without dry spots.

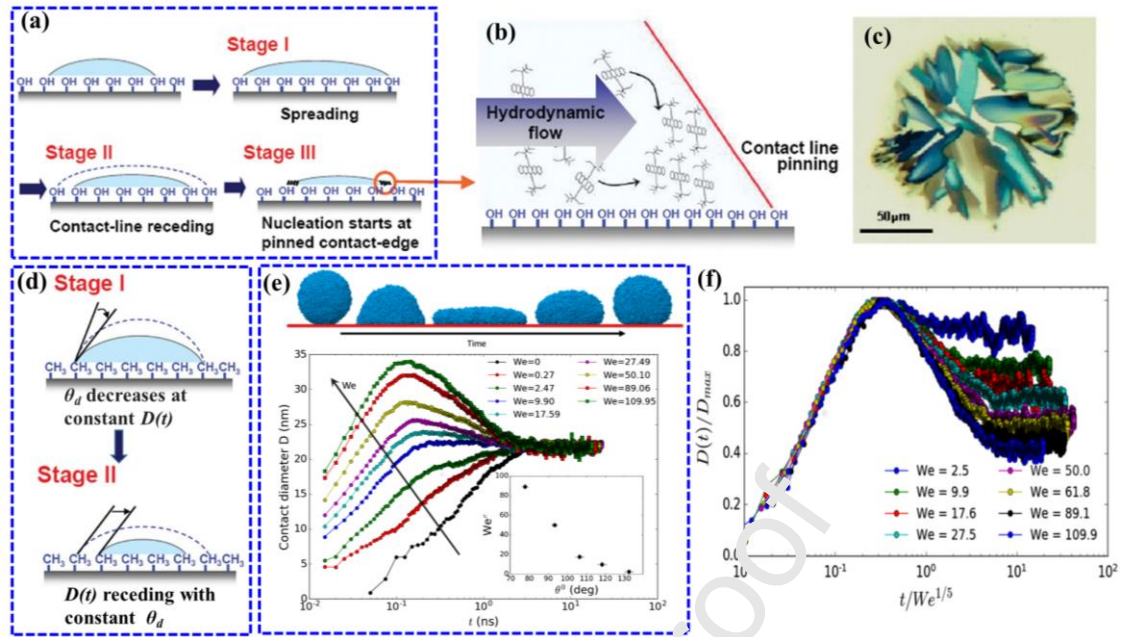


Fig. 20. (a) Schematic of a printed TIPS_PEN drop with three distinct stages on a hydrophilic substrate; (b) schematic of the TIPS_PEN molecules in the drying-mediated self-organization process near the contact line; (c) Optical microscopy images of inkjet-printed TIPS_PEN droplets on a hydrophilic substrate; (d) Schematic of a printed TIPS_PEN drop two distinct evaporation stages on a hydrophobic substrate. Reproduced with permission [218]. Copyright 2009, American Chemical Society. (e) The simulation snapshot for $C_{LS} = 0.4$ and $We = 109.9$ (We : Weber number) at different times (upper side), the dynamic drop contact diameter vs. time for the different We number for $C_{LS} = 0.6$ (lower side); (f) Collapsing data of $D(t)/D_{max}$ vs. $t/We^{-1/5}$ in a single curve. Reproduced with permission [215]. Copyright 2020, American Physical Society.

4.4. Other applications

In addition to the specific applications already described, dynamic wetting has

demonstrated important implications in coating, microfluids, textile dyeing, oil/water separation, detergency, soldering, etc. [220-223]. For example, dynamic wetting can be used to predict an optimal coating speed [61]. The increase of the driving force for wetting is accompanied by the decrease of the moving molecule mobility (*i.e.*, the reducing jump frequency κ^0) in the contact line region, and vice versa. The two opposing effects produced an optimal coating speed for the substrate with θ_0 around 122° . Water coating experiments are performed with the substrates containing various surfactants and the experimental results can well support the prediction. The results have a direct relevance to the efficiency and productivity in the coating industry. Given that the length of this review has to be limited, we cannot present all significant application works on dynamic wetting and it indeed presents some new fascinating application scenarios (like forensic science [224]).

5. Conclusions and outlooks

This review summarizes the recent advances of dynamic wetting from theoretical models, experiments, simulations and applications. The two main theoretical approaches for dynamic wetting that are MKT and HD approaches are discussed and compared with the focus on the fundamental difference on the channel of energy dissipations. Then combined models are also presented and analyzed. Subsequently, we discussed the representative behaviors of dynamic wetting for various types of liquids covering small-molecule liquids, metallic liquids, polymer liquids and simulated L-J liquids, where their interfacial physicochemical properties have been

highlighted. The described interfacial characteristics are interdisciplinary, which include, but are not limited to, the subject of interface science. It has revealed scientific importance and potential applications, making the topic of dynamic wetting a vibrant area both in the academic and industrial communities. Despite great efforts dedicated to the understanding of dynamic wetting, how to optimize the wetting research to improve industrial applications is still in its infancy. There are several challenges from fundamental to application that must be addressed before achieving that commercial goal. Therefore, in our humble opinion, some tentative suggestions and challenges are summarized as follows.

(1) There is still no consensus on the physical mechanism controlling dynamic wetting for a liquid on a substrate. The problem becomes increasingly complicated in the case of rough and/or chemically heterogeneous substrates or porous media due to contact angle hysteresis [44,225]. Therefore, the substrate should be, as far as possible, smooth and homogeneous, unless there is a particular purpose for exploring the effect of well-characterized roughness or heterogeneity [136,226,227]. Actually, the accurate characterization of wetting on a rough and/or heterogeneous substrate surface itself is an issue. From an experimental perspective, Liimatainen et al. [228] developed a scanning droplet adhesion microscopy with nN force resolution where the force sensitivity has several orders of magnitude better than current tensiometers and this apparatus is potentially an appropriate tool to map microscopic variations in surface texture and chemical composition of the substrate. From a theoretical perspective, new approaches to characterize wetting are highly necessary on non-ideal

surfaces, in addition to the well-known Wenzel model, Cassie-Baxter model and wicking state model. Recently, Sun et al. [229-231] proposed a new topological approach based on the Gauss-Bonnet theorem that yielded a robust and universal measure to characterize wetting on multiscale surfaces. In their approach, "deficit curvature" is defined to capture the effects of contact angle hysteresis and describe wetting in complex multiphase systems where wetting is difficult to quantify with traditional methods. These valuable experimental and theoretical works can help understand dynamic wetting, especially when the ubiquitous wetting hysteresis has to be taken into account.

(2) It is a vexed issue that whether the microscopic contact angle θ_m is velocity dependent or remains constant at the equilibrium value [40,52,55,67]. A constant θ_m is often assumed when analyzing dynamic wetting behavior since the variation of θ_m is experimentally difficult to access by the common optical microscopy techniques. Image optimization and processing methodologies remain an important topic to provide new insight into the behavior of the contact line at the nanoscale. In this regard, the nanoscale AFM investigation of wetting behavior is promising [232]. As far as we are aware, the θ_m variation of nonvolatile liquids has been revealed with sufficient resolution by AFM technique in opposition to one of the main hypotheses considered by the HD model [49,77,78]. However, the AFM is confined to nonvolatile liquids with exceedingly low contact line velocity in the order of nanometers per second [77] and the time resolution becomes another issue. Therefore, how to extend the state-of-the-art characterization techniques and experimental

set-ups to *in-situ* obtain interfacial information at nanoscale and appreciate the real physics of the moving contact line for the most common liquids at a regular velocity is urgently needed to help reveal the physical mechanism of dynamic wetting.

(3) Several researchers acknowledged that the hydrodynamic and frictional processes may be complementary and simultaneously play roles in dynamic wetting, producing the combined models [58-60,101]. It is generally accepted that high-viscosity liquids are dominated by viscous dissipation whereas the frictional dissipation is the main channel of dissipation for low-viscosity liquids [16,105]. However, the relationship between the viscous and frictional dissipations is not discussed at great depth in the combined models, as the theoretical foundations of the two dissipations are completely different. Furthermore, the understanding of how the two channels of energy dissipations switched remain rudimentary [105]. Therefore, more elaborated theoretical developments connecting viscous and frictional dissipations based on the existing combined models are still necessary.

(4) The molten polymers may be the most complex system for dynamic wetting due to their sensitivity to temperature, thermal stability, dispersity and possible chain reptation, etc. [233]. Yet, the relevant studies are able to uncover several particular physical characteristics (such as Kuhn segment length, surface segregation of short chains) [92,100]. Among them, surface segregation is a very interesting point. From an engineering perspective, the surface segregation may be relevant to the interfacial strength of fiber-reinforced polymer composites since more short polymer chains could tend to first contact and wet on the fiber/matrix interface during processing.

From a fundamental perspective, it is still a tough issue to *in situ* validate the surface segregation experimentally. A fluorescent labeled polymer melt could help monitor the dynamics of surface segregation [86,87].

(5) From a numerical simulation point of view, the concurrent multiscale simulations tackling simultaneously the atomistic details of interfaces by molecular dynamics (discrete approach) and the hydrodynamic of the liquid by computational fluid dynamics (continuum approach) should give us a comprehensive view of wetting dynamics, towards building a more general and robust model for dynamic wetting [234,235]. However, the way in which the 2 approaches should be linked both in spatial and temporal scales seems still debated and further progresses are required.

Declaration of Competing Interest

There are no conflicts to declare.

Acknowledgments

The authors gratefully acknowledge Dr. T.D. Blake for critical comments on this manuscript. This research has been partially funded by the National Natural Science Foundation of China (No. 52103036), Fundamental Research Funds for the Central Universities (No. SWU-KR22041) and the Interuniversity Attraction Poles Programme (IAP 7/38 MicroMAST) initiated by the Belgian Science Policy Office.

References

- [1] Barthlott W, Neinhuis C. Purity of the sacred lotus, or escape from contamination in biological surfaces. *Planta* 1997;202:1-8.
- [2] Gao X, Jiang L. Water-repellent legs of water striders. *Nature* 2004;432:36.
- [3] Parker AR, Lawrence CR. Water capture by a desert beetle. *Nature* 2001;414:33-4.
- [4] Zheng Y, Bai H, Huang Z, Tian X, Nie FQ, Zhao Y, et al. Directional water collection on wetted spider silk. *Nature* 2010;463:640-3.
- [5] Bai H, Ju J, Zheng Y, Jiang L. Functional fibers with unique wettability inspired by spider silks. *Adv Mater* 2012;24:2786-91.
- [6] Tian X, Chen Y, Zheng Y, Bai H, Jiang L. Controlling water capture of bioinspired fibers with hump structures. *Adv Mater* 2011;23:5486-91.
- [7] Liu M, Wang S, Jiang L. Nature-inspired superwettability systems. *Nat Rev Mater* 2017;2:17036.
- [8] Si Y, Yu C, Dong Z, Jiang L. Wetting and spreading: fundamental theories to cutting-edge applications. *Curr Opin Colloid Interface Sci* 2018;36:10-9.
- [9] Marengo M, De Coninck J. *The Surface Wettability Effect on Phase Change*. Cham, Switzerland: Springer; 2021.
- [10] de Gennes PG. Wetting: statics and dynamics. *Rev Mod Phys* 1985;57:827-63.
- [11] Eddi A, Winkels KG, Snoeijer JH. Short time dynamics of viscous drop spreading. *Phys Fluids* 2013;25:013102.
- [12] De Ruiter R, Colinet P, Brunet P, Snoeijer JH, Gekkerblom H. Contact line arrest in solidifying spreading drops. *Phys Rev Fluids* 2017;2:043602.
- [13] Chen X, Chen J, Ouyang X, Song Y, Xia K, Jiang P. Water droplet spreading and wicking on nanostructured surfaces. *Langmuir* 2017;33:701-7.
- [14] Wang X, Venzmer J, Bonaccorso E. Surfactant-enhanced spreading of sessile water drops on polypropylene surfaces. *Langmuir* 2016;32:7322-8.
- [15] Sauer BB, Kampert WG. Influence of viscosity on forced and spontaneous spreading: Wilhelmy fiber studies including practical methods for rapid viscosity measurement. *J Colloid Interface Sci* 1998;199:28-37.
- [16] Vega MJ, Seveno D, Lencour G, Adão MH, De Coninck J. Dynamics of the rise around a fiber: experimental evidence of the existence of several time scales. *Langmuir* 2005;21:9584-90.
- [17] Clanet C, Quéré D. Onset of menisci. *J Fluid Mech* 2002;460:131-49.
- [18] Zhmud B, Tiberghien P, Hallstensson K. Dynamics of capillary rise. *J Colloid Interface Sci* 2000;228:263-9.
- [19] Xue H, Fang Z, Yang Y, Huang J, Zhou L. Contact angle determined by spontaneous dynamic capillary rises with hydrostatic effects: Experiment and theory. *Chem Phys Lett* 2006;432:326-30.
- [20] O'Loughlin M, Wilk K, Priest C, Ralston J, Popescu M. Capillary rise dynamics of aqueous glycerol solutions in glass capillaries: A critical examination of the Washburn equation. *J Colloid Interface Sci* 2013;411:257-64.
- [21] Andruk T, Monaenkova D, Rubin B, Lee W-K, Kornev KG. Meniscus formation in a capillary and the role of contact line friction. *Soft Matter* 2014;10:609-15.
- [22] Grundke K, Uhlmann P, Gietzelt T, Redlich B, Jacobasch H-J. Studies on the wetting behaviour of polymer melts on solid surfaces using the Wilhelmy balance method. *Colloids Surf A* 1996;116:93-104.
- [23] Wang J, Fuentes CA, Zhang D, Wang X, Van Vuure AW, Seveno D. Wettability of carbon fibres at micro-and mesoscales. *Carbon* 2017;120:438-46.
- [24] Sauer BB, Dipaolo NV. Surface tension and dynamic wetting on polymers using the Wilhelmy

- method: Applications to high molecular weights and elevated temperatures. *J Colloid Interface Sci* 1991;144:527-37.
- [25] Blake TD, Dobson RA, Ruschak KJ. Wetting at high capillary numbers. *J Colloid Interface Sci* 2004;279:198-205.
- [26] Blake T, Shikhmurzaev Y. Dynamic wetting by liquids of different viscosity. *J Colloid Interface Sci* 2002;253:196-202.
- [27] Blake T, Batts G. The temperature-dependence of the dynamic contact angle. *J Colloid Interface Sci* 2019;553:108-16.
- [28] Vega MJ, Gouttiere C, Seveno D, Blake TD, Voué M, De Coninck J, et al. Experimental investigation of the link between static and dynamic wetting by forced wetting of nylon filament. *Langmuir* 2007;23:10628-34.
- [29] Blake T, Bracke M, Shikhmurzaev Y. Experimental evidence of nonlocal hydrodynamic influence on the dynamic contact angle. *Phys Fluids* 1999;11:1995-2007.
- [30] Mohammad Karim A, Suszynski WJ. Physics of dynamic contact line: hydrodynamics theory versus molecular kinetic theory. *Fluids* 2022;7:318.
- [31] Kuchin I, Starov V. Hysteresis of contact angle of sessile droplets on smooth homogeneous solid substrates via disjoining/conjoining pressure. *Langmuir* 2015;31:5245-52.
- [32] Kuchin IV, Starov VM. Hysteresis of the contact angle of a meniscus inside a capillary with smooth, homogeneous solid walls. *Langmuir* 2016;32:5333-40.
- [33] Arjmandi-Tash O, Kovalchuk NM, Trybala A, Kuchin IV, Starov V. Kinetics of wetting and spreading of droplets over various substrates. *Langmuir* 2017;33:4367-85.
- [34] Brutin D, Starov V. Recent advances in droplet wetting and evaporation. *Chem Soc Rev* 2018;47:558-85.
- [35] Ahmed G, Koursari N, Trybala A, Starov VM. Sessile droplets on deformable substrates. *Colloids Interfaces* 2018;2:56.
- [36] Wang H. From contact line structures to wetting dynamics. *Langmuir* 2019;35:10233-45.
- [37] Shikhmurzaev YD. Spreading of drops on solid surfaces in a quasi-static regime. *Phys Fluids* 1997;9:266-75.
- [38] Blake TD. The physics of moving wetting lines. *J Colloid Interface Sci* 2006;299:1-13.
- [39] Bonn D, Eggers J, Indekeu J, Meunier J, Rolley E. Wetting and spreading. *Rev Mod Phys* 2009;81:739-805.
- [40] Dussan E. On the spreading of liquids on solid surfaces: static and dynamic contact lines. *Annu Rev Fluid Mech* 1979;11:371-400.
- [41] De Coninck J, Blake TD. Wetting and molecular dynamics simulations of simple liquids. *Annu Rev Mater Res* 2008;38:1-22.
- [42] Lu G, Wang X-D, Duan Y-Y. A critical review of dynamic wetting by complex fluids: from Newtonian fluids to non-Newtonian fluids and nanofluids. *Adv Colloid Interface Sci* 2016;236:43-62.
- [43] Ralston J, Popescu M, Sedev R. Dynamics of wetting from an experimental point of view. *Annu Rev Mater Res* 2008;38:23-43.
- [44] Ramiasa M, Ralston J, Fetzer R, Sedev R. The influence of topography on dynamic wetting. *Adv Colloid Interface Sci* 2014;206:275-93.
- [45] Snoeijer JH, Andreotti B. Moving contact lines: scales, regimes, and dynamical transitions. *Annu Rev Fluid Mech* 2013;45:269-92.
- [46] Sedev R. The molecular-kinetic approach to wetting dynamics: achievements and limitations. *Adv*

Colloid Interface Sci 2015;222:661-9.

[47] Krawczyk J, Croce S, McLeish T, Chakrabarti B. Elasticity dominated surface segregation of small molecules in polymer mixtures. *Phys Rev Lett* 2016;116:208301.

[48] Fernandeztoledano JC, Blake TD, De Coninck J. Contact-line fluctuations and dynamic wetting. *J Colloid Interface Sci* 2019;540:322-9.

[49] Deng Y, Chen L, Liu Q, Yu J, Wang H. Nanoscale view of dewetting and coating on partially wetted solids. *J Phys Chem Lett* 2016;7:1763-8.

[50] Huh C, Scriven L. Hydrodynamic model of steady movement of a solid/liquid/fluid contact line. *J Colloid Interface Sci* 1971;35:85-101.

[51] Tanner L. The spreading of silicone oil drops on horizontal surfaces. *J Phys D: Appl Phys* 1979;12:1473.

[52] Voinov O. Hydrodynamics of wetting. *Fluid Dynamics* 1976;11:714-21.

[53] Blake TD, Haynes JM. Kinetics of liquid/liquid displacement. *J Colloid Interface Sci* 1969;30:421-3.

[54] Blake TD. Dynamic contact angles and wetting kinetics. In: Berg JC, (editor). *Wettability*. Vol. 49. New York: Marcel Dekker; 1993. Chapter 5. p. 251-309.

[55] Shikhmurzaev YD. The moving contact line on a smooth solid surface. *Int J Multiphase Flow* 1993;19:589-610.

[56] Shikhmurzaev YD. Moving contact lines in liquid/liquid/solid systems. *J Fluid Mech* 1997;334:211-49.

[57] Wu P, Nikolov A, Wasan D. Capillary dynamics driven by molecular self-layering. *Adv Colloid Interface Sci* 2017;243:114-20.

[58] Petrov P, Petrov I. A combined molecular-hydrodynamic approach to wetting kinetics. *Langmuir* 1992;8:1762-7.

[59] de Ruijter MJ, De Coninck J, Cshman G. Droplet spreading: partial wetting regime revisited. *Langmuir* 1999;15:2209-16.

[60] Brochard-Wyart F, de Gennes PG. Dynamics of partial wetting. *Adv Colloid Interface Sci* 1992;39:1-11.

[61] Blake TD, De Coninck J. The influence of solid-liquid interactions on dynamic wetting. *Adv Colloid Interface Sci* 2002;96:21-36.

[62] Rougier V, Cellier J, Gomina M, Bréard J. Slip transition in dynamic wetting for a generalized Navier boundary condition. *J Colloid Interface Sci* 2021;583:448-58.

[63] Wang X, Min Q, Zhang Z, Duan Y. Effect of Moving Contact Line's Curvature on Dynamic Wetting of non-Newtonian Fluids. *Langmuir* 2018;34:15612-20.

[64] Akai T, Bijeljic B, Blunt MJ. Wetting boundary condition for the color-gradient lattice Boltzmann method: Validation with analytical and experimental data. *Adv Water Resour* 2018;116:56-66.

[65] Cox R. The dynamics of the spreading of liquids on a solid surface. Part 1. Viscous flow. *J Fluid Mech* 1986;168:169-94.

[66] Petrov JG, Ralston J, Schneemilch M, Hayes RA. Dynamics of partial wetting and dewetting in well-defined systems. *J Phys Chem B* 2003;107:1634-45.

[67] Thompson PA, Robbins MO. Simulations of contact-line motion: slip and the dynamic contact angle. *Phys Rev Lett* 1989;63:766.

[68] de Gennes PG, Hervet H. Dynamique du mouillage: films précurseurs sur solide sec. *CR Acad Sci Paris* 1984;299:499.

- [69] Joanny J, Degennes P. Competition between wetting and adverse macroscopic forces. *C R Acad Sci Ser II* 1984;299:605-8.
- [70] Hocking L. A moving fluid interface on a rough surface. *J Fluid Mech* 1976;76:801-17.
- [71] Weidner D, Schwartz L. Contact-line motion of shear-thinning liquids. *Phys Fluids* 1994;6:3535-8.
- [72] Ansini L, Giacomelli L. Shear-thinning liquid films: macroscopic and asymptotic behaviour by quasi-self-similar solutions. *Nonlinearity* 2002;15:2147-64.
- [73] Carre A, Woehl P. Spreading of silicone oils on glass in two geometries. *Langmuir* 2006;22:134-9.
- [74] Sprenger M, Schlesener F, Dietrich S. Critical adsorption at chemically structured substrates. *Phys Rev E* 2005;71:056125.
- [75] Boudaoud A. Non-Newtonian thin films with normal stresses: dynamics and spreading. *Eur Phys J E* 2007;22:107-9.
- [76] Petrov JG, Ralston J, Schneemilch M, Hayes RA. Dynamics of partial wetting and dewetting of an amorphous fluoropolymer by pure liquids. *Langmuir* 2003;19:2795-801.
- [77] Chen L, Yu J, Wang H. Convex nanobending at a moving contact line: the missing mesoscopic link in dynamic wetting. *ACS Nano* 2014;8:11493-8.
- [78] Liu Q, Chen L, Deng Y, Wang H. Residual nano films and patterns formed by non-volatile liquid dewetting on smooth surfaces. *Chem Phys Lett* 2017;680:17-21.
- [79] de Gennes PG. Deposition of langmuir-blodgett layers. *Colloid Polym Sci* 1986;264:463-5.
- [80] Glasstone S, Laidler KJ, Eyring H. *The theory of rate processes*. New York: McGraw-Hill; 1941.
- [81] Duvivier D, Blake TD, De Coninck J. Toward a predictive theory of wetting dynamics. *Langmuir* 2013;29:10132-40.
- [82] Seveno D. *Dynamic wetting of fibers*. Mons: University of Mons; 2004.
- [83] Duvivier D, Seveno D, Rioboo R, Blake TD, De Coninck J. Experimental evidence of the role of viscosity in the molecular kinetic theory of dynamic wetting. *Langmuir* 2011;27:13015-21.
- [84] Blake T, De Coninck J. Dynamics of wetting and Kramers' theory. *Eur Phys J Special Topics* 2011;197:249-64.
- [85] Léger L, Hervet H, Masse G, Durliat E. Wall slip in polymer melts. *J Phys: Condens Matter* 1997;9:7719.
- [86] Hénot M, Chennevière A, Drockenmuller E, Léger L, Restagno F. Comparison of the slip of a PDMS melt on weakly adsorbing surfaces measured by a new photobleaching-based technique. *Macromolecules* 2017;50:5592-8.
- [87] Hénot M, Grzella M, Zhang J, Mariot S, Antoniuk I, Drockenmuller E, et al. Temperature-controlled slip of polymer melts on ideal substrates. *Phys Rev Lett* 2018;121:177802.
- [88] Sabzevari SM, Cohen I, Wood-Adams PM. Wall slip of bidisperse linear polymer melts. *Macromolecules* 2014;47:3154-60.
- [89] Blake TD, Fernandez-Toledano JC, Doyen G, De Coninck J. Forced wetting and hydrodynamic assist. *Phys Fluids* 2015;27:112101.
- [90] Hoffman RL. A study of the advancing interface. I. Interface shape in liquid—gas systems. *J Colloid Interface Sci* 1975;50:228-41.
- [91] Seveno D, Vaillant A, Rioboo R, Adao H, Conti J, De Coninck J. Dynamics of wetting revisited. *Langmuir* 2009;25:13034-44.
- [92] Zhang Y, Fuentes CA, Koekoekx R, Clasen C, Van Vuure AW, De Coninck J, et al. Spreading dynamics of molten polymer drops on glass substrates. *Langmuir* 2017;33:8447-54.
- [93] Paneru M, Priest C, Sedev R, Ralston J. Static and dynamic electrowetting of an ionic liquid in a

- solid/liquid/liquid system. *J Am Chem Soc* 2010;132:8301-8.
- [94] Davis MJ, Davis SH. Droplet spreading: Theory and experiments. *Comptes Rendus Physique* 2013;14:629-35.
- [95] Mohammad Karim A, Davis S, Kavehpour HP. Forced versus spontaneous spreading of liquids. *Langmuir* 2016;32:10153-8.
- [96] Pucci MF, Duchemin B, Gomina M, Bréard J. Temperature effect on dynamic wetting of cellulosic substrates by molten polymers for composite processing. *Compos Part A-Appl Sci Manuf* 2018;114:307-15.
- [97] Li R, Manica R, Yeung A, Xu Z. Spontaneous displacement of high viscosity micron size oil droplets from a curved solid in aqueous solutions. *Langmuir* 2019;35:615.
- [98] Li R, Manica R, Lu Y, Xu Z. Role of surfactants in spontaneous displacement of high viscosity oil droplets from solid surfaces in aqueous solutions. *J Colloid Interface Sci* 2020;579:898-908.
- [99] Quéré D, Di Meglio J-M. The meniscus on a fibre. *Adv Colloid Interface Sci* 1994;48:141-50.
- [100] Zhang Y, Vandaele A, Seveno D, De Coninck J. Wetting dynamics of polydimethylsiloxane mixtures on a poly(ethylene terephthalate) fiber. *J Colloid Interface Sci* 2018;525:243-50.
- [101] Seveno D, De Coninck J. Possibility of different time scales in the capillary rise around a fiber. *Langmuir* 2004;20:737-42.
- [102] Martic G, Gentner F, Seveno D, De Coninck J, Blake TD. The possibility of different time scales in the dynamics of pore imbibition. *J Colloid Interface Sci* 2004;270:171-9.
- [103] Cazabat AM, Cohen Stuart MA. Dynamics of wetting: effects of surface roughness. *J Phys Chem* 1986;90:5845-9.
- [104] Soleymaniha M, Felts JR. Measurement of nanoscale molten polymer droplet spreading using atomic force microscopy. *Rev Sci Instrum* 2018;89:033703.
- [105] Zhang Y, Moins S, Coulembier O, Seveno D, De Coninck J. Capillary rise of polydimethylsiloxane around a poly(ethylene terephthalate) fiber versus viscosity: existence of a sharp transition in the dynamic wetting behavior. *J Colloid Interface Sci* 2019;536:499-506.
- [106] de Ruijter M, Kölsch P, Voué M, De Coninck J, Rabe J. Effect of temperature on the dynamic contact angle. *Colloids Surf A* 1998;144:235-43.
- [107] Ausserré D, Picard A, Léger L. Existence and role of the precursor film in the spreading of polymer liquids. *Phys Rev Lett* 1986;57:2671.
- [108] de Ruijter MJ, Charlot M, Voué M, De Coninck J. Experimental evidence of several time scales in drop spreading. *Langmuir* 2000;16:2363-8.
- [109] Washburn EW. The dynamics of capillary flow. *Phys Rev* 1921;17:273.
- [110] Yao Y, Butt HJ, Floudas G, Zhou J, Doi M. Theory on capillary filling of polymer melts in nanopores. *Macromol Rapid Commun* 2018;1800087.
- [111] Ranabothu SR, Karnezis C, Dai LL. Dynamic wetting: hydrodynamic or molecular-kinetic? *J Colloid Interface Sci* 2005;288:213-21.
- [112] Fernández-Toledano J, Blake T, De Coninck J. Taking a closer look: A molecular-dynamics investigation of microscopic and apparent dynamic contact angles. *J Colloid Interface Sci* 2021;587:311-23.
- [113] Blake TD, Fernández-Toledano J, De Coninck J. A possible way to extract the dynamic contact angle at the molecular scale from that measured experimentally. *J Colloid Interface Sci* 2023;629:660-9.
- [114] De Coninck J, de Ruijter MJ, Voué M. Dynamics of wetting. *Curr Opin Colloid Interface Sci*

2001;6:49-53.

[115] Saiz E, Tomsia A, Rauch N, Scheu C, Rühle M, Benhassine M, et al. Nonreactive spreading at high temperature: molten metals and oxides on molybdenum. *Phys Rev E* 2007;76:041602.

[116] Heshmati M, Piri M. Experimental investigation of dynamic contact angle and capillary rise in tubes with circular and noncircular cross sections. *Langmuir* 2014;30:14151-62.

[117] Eggers J, Evans R. Comment on “Dynamic wetting by liquids of different viscosity,” by TD Blake and YD Shikhmurzaev. *J Colloid Interface Sci* 2004;280:537-8.

[118] Shikhmurzaev YD, Blake TD. Response to the comment on [J. Colloid Interface Sci. 253 (2002) 196] by J. Eggers and R. Evans. *J Colloid Interface Sci* 2004;280:539-41.

[119] Wu P, Nikolov AD, Wasan DT. Capillary rise: Validity of the dynamic contact angle models. *Langmuir* 2017;33:7862-72.

[120] Wang Z, Orejon D, Takata Y, Sefiane K. Wetting and evaporation of multicomponent droplets. *Phys Rep* 2022;960:1-37.

[121] Nikolayev VS. Evaporation effect on the contact angle and contact line dynamics. In: Marengo M, De Coninck J, (editors). *The Surface Wettability Effect on Phase Change*. Switzerland: Springer; 2022. Chapter 6. p. 133-87.

[122] Biance AL, Clanet C, Quéré D. First steps in the spreading of a liquid droplet. *Phys Rev E* 2004;69:016301.

[123] Winkels KG, Weijs JH, Eddi A, Snoeijer JH. Initial spreading of low-viscosity drops on partially wetting surfaces. *Phys Rev E* 2012;85:055301.

[124] Qiu S, Fuentes CA, Zhang D, Van Vuure AW, Seveno D. Wettability of a single carbon fiber. *Langmuir* 2016;32:9697-705.

[125] Qiu S, Wang J, Zhang D, Van Vuure AW, Seveno D, Fuentes CA. Wetting dynamics and surface energy components of single carbon fibers. *J Colloid Interface Sci* 2019;557:349-56.

[126] Stalcup EJ, Seemann R, Herminghaus S, Law BM. Dissipation mechanisms in ionic liquids. *J Colloid Interface Sci* 2009;338:523-8.

[127] Delcheva I, Beattie D, Ralston J, Krasowska M. Dynamic wetting of imidazolium-based ionic liquids on gold and glass. *Phys Chem Chem Phys* 2018;20:2084-93.

[128] Li H, Sedev R, Ralston J. Dynamic wetting of a fluoropolymer surface by ionic liquids. *Phys Chem Chem Phys* 2011;13:3912-9.

[129] Delcheva I, Ralston J, Beattie DA, Krasowska M. Static and dynamic wetting behaviour of ionic liquids. *Adv Colloid Interface Sci* 2015;222:162-71.

[130] Tsuchitani S, Fukutake T, Mukai D, Miki H, Kikuchi K. Unstable spreading of ionic liquids on an aqueous substrate. *Langmuir* 2017;33:11040-6.

[131] Shiimoto S, Higuchi H, Yamaguchi K, Takaba H, Kobayashi M. Spreading dynamics of a precursor film of ionic liquid or water on a micropatterned polyelectrolyte brush surface. *Langmuir* 2021;37:3049-56.

[132] Farajzadeh R, Andrianov A, Krastev R, Hirasaki G, Rossen WR. Foam–oil interaction in porous media: Implications for foam assisted enhanced oil recovery. *Adv Colloid Interface Sci* 2012;183:1-13.

[133] Mitra S, Mitra SK. Understanding the early regime of drop spreading. *Langmuir* 2016;32:8843-8.

[134] Bazazi P, Sanati-Nezhad A, Hejazi SH. Wetting dynamics in two-liquid systems: Effect of the surrounding phase viscosity. *Phys Rev E* 2018;97:063104.

[135] Ramiasa M, Ralston J, Fetzer R, Sedev R. Contact line friction in liquid–liquid displacement on hydrophobic surfaces. *J Phys Chem C* 2011;115:24975-86.

- [136] Ramiasa M, Ralston J, Fetzner R, Sedev R, Fopp-Spori DM, Morhard C, et al. Contact line motion on nanorough surfaces: A thermally activated process. *J Am Chem Soc* 2013;135:7159-71.
- [137] Xiang B, Li R, Liu B, Manica R, Liu Q. Effect of sodium citrate and calcium ions on the spontaneous displacement of heavy oil from quartz surfaces. *J Phys Chem C* 2020;124:20991-7.
- [138] Tian W, Wu K, Chen Z, Lei Z, Gao Y, Chen Z, et al. Dynamic wetting of solid-liquid-liquid system by molecular kinetic theory. *J Colloid Interface Sci* 2020;579:470-8.
- [139] Goossens S, Seveno D, Rioboo R, Vaillant A, Conti J, De Coninck J. Can we predict the spreading of a two-liquid system from the spreading of the corresponding liquid-air systems? *Langmuir* 2011;27:9866-72.
- [140] Seveno D, Blake TD, Goossens S, De Coninck J. Predicting the wetting dynamics of a two-liquid system. *Langmuir* 2011;27:14958-67.
- [141] Seveno D, Blake TD, Goossens S, De Coninck J. Correction to “predicting the wetting dynamics of a two-liquid system”. *Langmuir* 2018;34:5160-1.
- [142] Li R, Lu Y, Manica R. Spreading and receding of oil droplets on silanized glass surfaces in water: Role of three-phase contact line flow direction in spontaneous displacement. *J Colloid Interface Sci* 2021;587:672-82.
- [143] Venzmer J. Superspreading—20 years of physicochemical research. *Curr Opin Colloid Interface Sci* 2011;16:335-43.
- [144] Theodorakis PE, Smith ER, Müller EA. Spreading of aqueous droplets with common and superspreading surfactants. A molecular dynamics study. *Colloids Surf A* 2019;581:123810.
- [145] Venzmer J. Superspreading—Has the mystery been unraveled? *Adv Colloid Interface Sci* 2021;288:102343.
- [146] Kovalchuk NM, Simmons MJ. Surfactant-mediated wetting and spreading: Recent advances and applications. *Curr Opin Colloid Interface Sci* 2021;51:101375.
- [147] Nikolov AD, Wasan DT, Wu P. Marangoni flow alters wetting: Coffee ring and superspreading. *Curr Opin Colloid Interface Sci* 2021;51:101387.
- [148] Theodorakis PE, Müller EA, Craster RV, Matar OK. Insights into surfactant-assisted superspreading. *Curr Opin Colloid Interface Sci* 2014;19:283-9.
- [149] Rafaï S, Sarker D, Bergeron V, Meunier J, Bonn D. Superspreading: aqueous surfactant drops spreading on hydrophobic surfaces. *Langmuir* 2002;18:10486-8.
- [150] Lin J, Wang W, Li W, Zhu M, Zheng C, Liu Z, et al. A gemini-type superspreader: Synthesis, spreading behavior and superspreading mechanism. *Chem Eng J* 2017;315:262-73.
- [151] Saiz E, Tomsia AP. Kinetics of high-temperature spreading. *Curr Opin Solid State Mater Sci* 2005;9:167-73.
- [152] Kumar G, Prabhu KN. Review of non-reactive and reactive wetting of liquids on surfaces. *Adv Colloid Interface Sci* 2007;133:61-89.
- [153] Wu M, Chang L, Zhang L, He X, Qu X. Effects of roughness on the wettability of high temperature wetting system. *Surf Coat Technol* 2016;287:145-52.
- [154] Eustathopoulos N, Nicholas MG, Drevet B. Wettability at high temperatures: Elsevier; 1999.
- [155] Protsenko P, Garandet J-P, Voytovych R, Eustathopoulos N. Thermodynamics and kinetics of dissolutive wetting of Si by liquid Cu. *Acta Mater* 2010;58:6565-74.
- [156] Lin Q, Xie K, Sui R, Mu D, Cao R, Chang J, et al. Kinetic analysis of wetting and spreading at high temperatures: A review. *Adv Colloid Interface Sci* 2022;305:102698.
- [157] Lopez-Esteban S, Saiz E, Moya JS, Tomsia AP. Spreading of viscous liquids at high temperature:

- Silicate glasses on molybdenum. *Langmuir* 2005;21:2438-46.
- [158] Benhassine M, Saiz E, Tomsia A, De Coninck J. Role of substrate commensurability on non-reactive wetting kinetics of liquid metals. *Acta Mater* 2010;58:2068-78.
- [159] Kai X, Tian K, Wang C, Jiao L, Chen G, Zhao Y. Effects of ultrasonic vibration on the microstructure and tensile properties of the nano ZrB₂/2024Al composites synthesized by direct melt reaction. *J Alloys Compd* 2016;668:121-7.
- [160] Zhao J, Wu X, Ning L, Zhang J, Han C, Li Y. Wetting of aluminium and carbon interface during preparation of Al-Ti-C grain refiner under ultrasonic field. *Ultrason Sonochem* 2021:105633.
- [161] Jiang T-S, Soo-Gun O, Slattery JC. Correlation for dynamic contact angle. *J Colloid Interface Sci* 1979;69:74-7.
- [162] Saiz E, Tomsia AP. Atomic dynamics and Marangoni films during liquid-metal spreading. *Nat Mater* 2004;3:903-9.
- [163] Li Y, Wang Z, Long W, Lei M, Hu X. Wetting kinetics and spreading phenomena of Sn-35Bi-1Ag solder on different substrates. *J Mater Sci Mater Electron* 2018;29:13014-24.
- [164] Sun Q, Jin P, Liu Y, Li J, Wang J, Ma T, et al. Wetting of liquid copper on TC4 titanium alloy and 304 stainless steel at 1273–1433 K. *Mater Des* 2019;169:107667.
- [165] Wang F, Reiter A, Kellner M, Brillo J, Selzer M, Nettle B. Phase-field modeling of reactive wetting and growth of the intermetallic Al₂Au phase in the Al-Au system. *Acta Mater* 2018;146:106-18.
- [166] Sun Y, Yousefi E, Kunwar A, Moelans N, Severo J, Guo M. Study of the interfacial reactions controlling the spreading of Al on Ni. *Appl Surf Sci* 2022;571:151272.
- [167] Shi J, Wang Q, Tian F, Zhang L, Zhang X. Reactive wetting and interfacial reaction mechanism of ZrC-SiC ceramic and Ag-Zr filler. *J Eur Ceram Soc* 2021;41:7464-8.
- [168] Ramos-Masana A, Colominas C. Evaluation of DC-MS and HiPIMS TiB₂ and TaN coatings as diffusion barriers against molten aluminium. An insight into the wetting mechanism. *Surf Coat Technol* 2019;375:171-81.
- [169] Eustathopoulos N. Dynamics of wetting in reactive metal/ceramic systems. *Acta Mater* 1998;46:2319-27.
- [170] Aksay IA, Hoge CL, Pask JA. Wetting under chemical equilibrium and nonequilibrium conditions. *J Phys Chem* 1974 78:1178-83.
- [171] Loehman R, Hosking R, Gauntt B, Kotula P, Lu P. Reactions of Hf-Ag and Zr-Ag alloys with Al₂O₃ at elevated temperatures. *J Mater Sci* 2005;40:2319-24.
- [172] Dezellus O, Hodaj F, Eustathopoulos N. Progress in modelling of chemical-reaction limited wetting. *J Eur Ceram Soc* 2003;23:2797-803.
- [173] Eustathopoulos N, Voytovych R. The role of reactivity in wetting by liquid metals: a review. *J Mater Sci* 2016;51:425-37.
- [174] Schonhorn H, Frisch H, Kwei T. Kinetics of wetting of surfaces by polymer melts. *J Appl Phys* 1966;37:4967-73.
- [175] Newman S. Kinetics of wetting of surfaces by polymers; capillary flow. *J Colloid Interface Sci* 1968;26:209-13.
- [176] Cherry B, Holmes C. Kinetics of wetting of surfaces by polymers. *J Colloid Interface Sci* 1969;29:174-6.
- [177] Zhang Y. *Wetting Dynamics of Liquid Polymers*: KU Leuven; 2019.
- [178] Chiappori C, Russo S, Turturro A, Passerone A, Sangiorgi R. Wettability of glass substrates by

- molten nylon-6. *Polymer* 1981;22:534-8.
- [179] Rwei S-P, Hung Su S. Unsteady-state contact angle on interface between polymer melt and TiO₂. *Compos Interfaces* 2008;15:351-61.
- [180] Bex GJ, Seveno D, De Keyzer J, Desplentere F, Van Bael A. Wetting measurements as a tool to predict the thermoplastic/thermoset rubber compatibility in two-component injection molding. *J Appl Polym Sci* 2018;135:46046.
- [181] Rubinstein M, Colby RH. *Polymer physics*. Oxford, U.K.: Oxford University Press; 2003.
- [182] Sauret A, Boulogne F, Cébron D, Dressaire E, Stone HA. Wetting morphologies on an array of fibers of different radii. *Soft Matter* 2015;11:4034-40.
- [183] Peters BL, Salerno KM, Ge T, Perahia D, Grest GS. Effect of Chain Length Dispersity on the Mobility of Entangled Polymers. *Phys Rev Lett* 2018;121:057802.
- [184] Yao Y, Butt H-J, Zhou J, Doi M, Floudas G. Capillary Imbibition of Polymer Mixtures in Nanopores. *Macromolecules* 2018;51:3059-65.
- [185] Geoghegan M, Krausch G. Wetting at polymer surfaces and interfaces. *Prog Polym Sci* 2003;28:261-302.
- [186] Sabattié EF, Tasche J, Wilson MR, Skoda MW, Hughes A, Lindner T, et al. Predicting oligomer/polymer compatibility and the impact on nanoscale segregation in thin films. *Soft Matter* 2017;13:3580-91.
- [187] Jones RAL, Kramer EJ, Rafailovich MH, Sokolov J, Schwarz SA. Surface Enrichment in an Isotopic Polymer Blend. *Phys Rev Lett* 1989;62:280-3.
- [188] Steiner U, Klein J, Eiser E, Budkowski A, Fetters LJ. Complete wetting from polymer mixtures. *Science* 1992;258:1126-.
- [189] Brooks CF, Grillet AM, Emerson JA. Experimental investigation of the spontaneous wetting of polymers and polymer blends. *Langmuir* 2006;22:9928-41.
- [190] Lee E, Müller-Plathe F. Effect of polymer on the contact line friction of a capillary bridge. *Macromolecules* 2022;55:2649-58.
- [191] Koplik J, Banavar JR, Willemson JF. Molecular dynamics of Poiseuille flow and moving contact lines. *Phys Rev Lett* 1988;60:1282-5.
- [192] Thompson PA, Robbins MO. Simulations of contact-line motion: Slip and the dynamic contact angle. *Phys Rev Lett* 1989;63:766-9.
- [193] Bekele S, Evans OG, Tsige M. Spreading dynamics of water droplets on a completely wetting surface. *J Phys Chem C* 2020;124:20109-15.
- [194] De Coninck J, D'Ortona U, Koplik J, Banavar JR. Terraced spreading of chain molecules via molecular dynamics. *Phys Rev Lett* 1995;74:928.
- [195] Kim SJ, Kim J, Moon M-W, Lee K-R, Kim H-Y. Experimental study of drop spreading on textured superhydrophilic surfaces. *Phys Fluids* 2013;25:092110.
- [196] Fernández-Toledano J-C, Blake T, De Coninck J. Moving contact lines and Langevin formalism. *J Colloid Interface Sci* 2020;562:287-92.
- [197] Fernández-Toledano JC, Blake TD, De Coninck J, Kanduč M. Hidden microscopic life of the moving contact line of a waterlike liquid. *Phys Rev Fluids* 2020;5:104004.
- [198] Wang S, Liu K, Yao X, Jiang L. Bioinspired surfaces with superwettability: new insight on theory, design, and applications. *Chem Rev* 2015;115:8230-93.
- [199] Mohammad Karim A. A review of physics of moving contact line dynamics models and its applications in interfacial science. *J Appl Phys* 2022;132:080701.

- [200] Duez C, Ybert C, Clanet C, Bocquet L. Wetting controls separation of inertial flows from solid surfaces. *Phys Rev Lett* 2010;104:084503.
- [201] Dong Z, Wu L, Wang J, Ma J, Jiang L. Superwettability controlled overflow. *Adv Mater* 2015;27:1745-50.
- [202] Keller JB. Teapot effect. *J Appl Phys* 1957;28:859-64.
- [203] Andrews H, Eccles E, Schofield W, Badyal J. Three-dimensional hierarchical structures for fog harvesting. *Langmuir* 2011;27:3798-802.
- [204] Bai H, Ju J, Sun R, Chen Y, Zheng Y, Jiang L. Controlled fabrication and water collection ability of bioinspired artificial spider silks. *Adv Mater* 2011;23:3708-11.
- [205] Zhai L, Berg MC, Cebeci FC, Kim Y, Milwid JM, Rubner MF, et al. Patterned superhydrophobic surfaces: toward a synthetic mimic of the Namib Desert beetle. *Nano Lett* 2006;6:1213-7.
- [206] Dorrer C, Rühle J. Mimicking the *Stenocara* beetle—dewetting of drops from a patterned superhydrophobic surface. *Langmuir* 2008;24:6154-8.
- [207] Fernández-Toledano JC, Fagniard C, Conti G, De Coninck J, Dunlop F, Huillet T. Optimizing fog harvesting by biomimicry. *Phys Rev Fluids* 2022;7:033604.
- [208] Gao N, Chiu M, Neto C. Receding contact line motion on nanopatterned and micropatterned polymer surfaces. *Langmuir* 2017;33:12602-8.
- [209] Al-Khayat O, Hong JK, Beck DM, Minett AI, Neto C. Patterned polymer coatings increase the efficiency of dew harvesting. *ACS Appl Mater Interfaces* 2017;9:13676-84.
- [210] Thickett SC, Neto C, Harris AT. Biomimetic surface coatings for atmospheric water capture prepared by dewetting of polymer films. *Adv Mater* 2011;23:3718-22.
- [211] Leach R, Stevens F, Langford S, Dickinson J. Dropwise condensation: experiments and simulations of nucleation and growth of water droplets in a cooling system. *Langmuir* 2006;22:8864-72.
- [212] Tian D, Song Y, Jiang L. Patterning of controllable surface wettability for printing techniques. *Chem Soc Rev* 2013;42:5184-209.
- [213] Hail CU, Höller C, Matsuzaki K, Köhner P, Renger J, Sandoghdar V, et al. Nanoprinting organic molecules at the quantum level. *Nat Commun* 2019;10:1-8.
- [214] Wen L, Tian Y, Jiang L. Bioinspired super-wettability from fundamental research to practical applications. *Angew Chem Int Ed* 2015;54:3387-99.
- [215] Fernández-Toledano JC, Braeckeveldt B, Marengo M, De Coninck J. How wettability controls nanoprinting. *Phys Rev Lett* 2020;124:224503.
- [216] Leopoldes J, Dupuis A, Bucknall D, Yeomans J. Jetting micron-scale droplets onto chemically heterogeneous surfaces. *Langmuir* 2003;19:9818-22.
- [217] Kusumaatmaja H, Léopoldès J, Dupuis A, Yeomans JM. Drop dynamics on chemically patterned surfaces. *Europhys Lett* 2006;73:740-6.
- [218] Lim J, Lee W, Kwak D, Cho K. Evaporation-induced self-organization of inkjet-printed organic semiconductors on surface-modified dielectrics for high-performance organic transistors. *Langmuir* 2009;25:5404-10.
- [219] Park YD, Lim JA, Lee HS, Cho K. Interface engineering in organic transistors. *Mater Today* 2007;10:46-54.
- [220] Zhang B, Song W, Guo H. Wetting, infiltration and interaction behavior of CMAS towards columnar YSZ coatings deposited by plasma spray physical vapor. *J Eur Ceram Soc* 2018;38:3564-72.
- [221] Wang S, Wang T, Ge P, Xue P, Ye S, Chen H, et al. Controlling flow behavior of water in microfluidics with a chemically patterned anisotropic wetting surface. *Langmuir* 2015;31:4032-9.

- [222] Chu Z, Feng Y, Seeger S. Oil/water separation with selective superantiwetting/superwetting surface materials. *Angew Chem Int Ed Engl* 2015;54:2328-38.
- [223] Wang J, Wu Y, Chen W, Xie Y. Wetting behavior of eutectic Au–Sn solder on Ni/Au metallization at different temperatures. *J Mater Sci Mater Electron* 2022;33:1774-82.
- [224] Smith F, Brutin D. Wetting and spreading of human blood: Recent advances and applications. *Curr Opin Colloid Interface Sci* 2018;36:78-83.
- [225] McClure JE, Armstrong RT, Berrill MA, Schlüter S, Berg S, Gray WG, et al. Geometric state function for two-fluid flow in porous media. *Phys Rev Fluids* 2018;3:084306.
- [226] Ramiasa M, Ralston J, Fetzer R, Sedev R. Nanoroughness Impact on Liquid–Liquid Displacement. *J Phys Chem C* 2012;116:10934-43.
- [227] Karim AM, Rothstein JP, Kavehpour HP. Experimental study of dynamic contact angles on rough hydrophobic surfaces. *J Colloid Interface Sci* 2018;513:658-65.
- [228] Liimatainen V, Vuckovac M, Jokinen V, Sariola V, Hokkanen M, Zhou Q, et al. Mapping microscale wetting variations on biological and synthetic water-repellent surfaces. *Nat Commun* 2017;8:1798.
- [229] Sun C, McClure JE, Mostaghimi P, Herring AL, Berg S, Armstrong RT. Probing effective wetting in subsurface systems. *Geophys Res Lett* 2020;47:1-10.
- [230] Sun C, McClure JE, Mostaghimi P, Herring AL, Meisenheimer DE, Wildenschild D, et al. Characterization of wetting using topological principles. *J Colloid Interface Sci* 2020;578:106-15.
- [231] Sun C, McClure J, Berg S, Mostaghimi P, Armstrong RT. Universal description of wetting on multiscale surfaces using integral geometry. *J Colloid Interface Sci* 2022;608:2330-8.
- [232] Savulescu G, Rücker M, Scanziani A, Pini R, Georgiadis A, Luckham P. Atomic force microscopy for the characterisation of pinning effects of seawater micro-droplets in n-decane on a calcite surface. *J Colloid Interface Sci* 2021;592:397-404.
- [233] Zhang Y, Zhang H, Guo M, De Coninck J, Seveno D. Reactive spreading dynamics of molten polymer liquids. *Macromolecules* 2022. DOI: 10.1021/acs.macromol.2c02530.
- [234] Wu H, Fichthorn KA, Gomon A. An atomistic–continuum hybrid scheme for numerical simulation of droplet spreading on a solid surface. *Heat Mass Transfer* 2014;50:351-61.
- [235] Afkhami S. Challenges of numerical simulation of dynamic wetting phenomena: a review. *Curr Opin Colloid Interface Sci* 2022;57:101523.

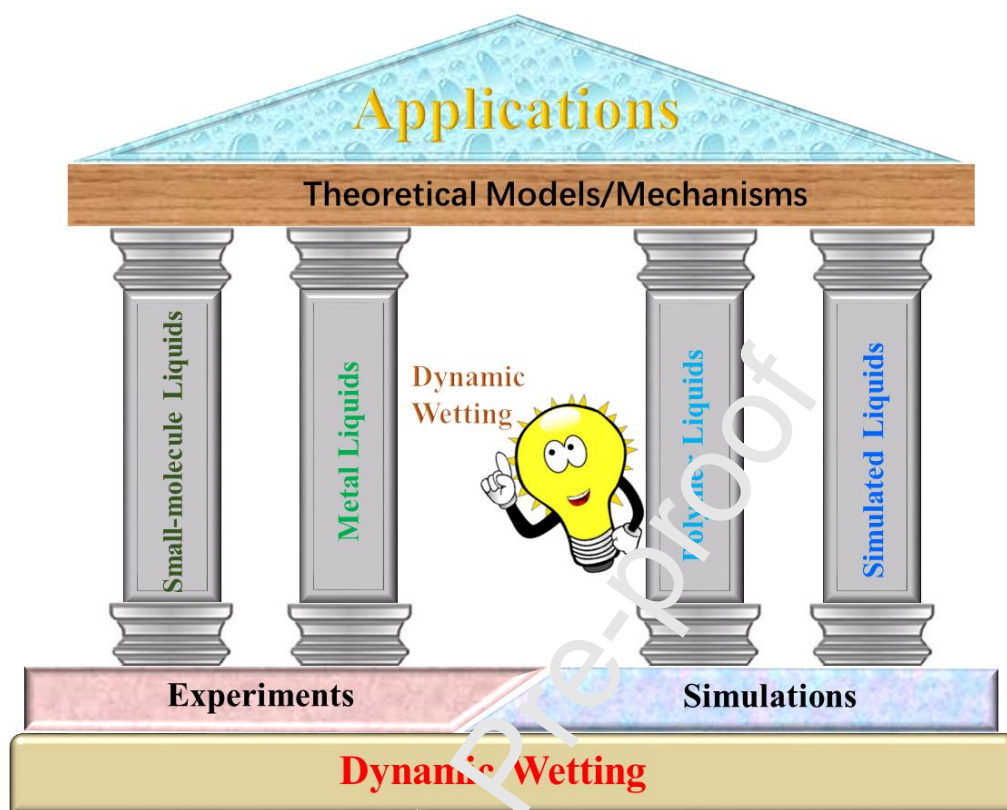
Declaration of interests

The authors declare that they have no known competing financial interests or personal relationships that could have appeared to influence the work reported in this paper.

The authors declare the following financial interests/personal relationships which may be considered as potential competing interests:

Journal Pre-proof

Graphical Abstracts



Highlights

1. The theoretical models of dynamic wetting are presented and critically compared.
2. The dynamic wetting of various liquids ranging from small-molecule liquids to simulated liquids are systematically summarized.
3. The suitability of the theoretical models is examined and discussed.
4. The new physical concepts (such as surface segregation, contact line fluctuations, etc.) are particularly discussed.
5. The cutting-edge applications are presented and some tentative suggestions and challenges are proposed.